

New measurement of the Boltzmann constant k by acoustic thermometry of helium-4 gas

L Pitre^{1,8}, F Sparasci¹, L Risegari¹, C Guianvarc'h¹, C Martin¹, M E Himbert¹, M D Plimmer¹, A Allard²,
B Marty³, P A Giuliano Albo⁴, B Gao⁵, M R Moldover⁶ and J B Mehl⁷

¹LCM-LNE Cnam, 61 rue du Landy, F93210 La Plaine-St Denis, France

²LNE, 29 rue Roger Hennequin, F78197 Trappes, France

³CRPG-CNRS, UMR 7358, 15 rue Notre Dame des Pauvres, 54500 Vandoeuvre-lès-Nancy

⁴Istituto Nazionale di Ricerca Metrologica, Thermodynamics Division, strada delle Cacce, 91 10135 Torino, Italy

⁵Technical Institute of Physics and Chemistry, Chinese Academy of Sciences,
29 Zhongguancun East Road, Haidian District, Beijing 100190, People's Republic of China

⁶Sensor Science Division, National Institute of Standards and Technology, Gaithersburg, MD,
United States of America

⁷36 Zunuqua Trail, P.O. Box 307, Orcas, WA 98280-0307, United States of America

⁸Corresponding author E-mail: laurent.pitre@cnam.fr

Received 8 May 2017, revised 26 June 2017

Accepted for publication 27 June 2017

Published 11 October 2017

Abstract

The SI unit of temperature will soon be redefined in terms of a fixed value of the Boltzmann constant k derived from an ensemble of measurements worldwide. We report on a new determination of k using acoustic thermometry of helium-4 gas in a 3 l volume quasi-spherical resonator. The method is based on the accurate determination of acoustic and microwave resonances to measure the speed of sound at different pressures. We find for the universal gas constant $R=8.3144614(50) \text{ J}\cdot\text{mol}^{-1}\cdot\text{K}^{-1}$. Using the current best available value of the Avogadro constant, we obtain $k=1.38064878(83)\times 10^{-23} \text{ J}\cdot\text{K}^{-1}$ with $u(k)/k = 0.60\times 10^{-6}$, where the uncertainty u is one standard uncertainty corresponding to a 68 % confidence level. This value is consistent with our previous determinations and with that of the 2014 CODATA adjustment of the fundamental constants (Mohr *et al.*, *Rev. Mod. Phys.* **88**, 035009 (2016)), within the standard uncertainties. We combined the present values of k and $u(k)$ with earlier values that were measured at LNE. Assuming the maximum possible correlations between the measurements, $(k_{\text{present}}/k - 1) = 0.07 \times 10^{-6}$ and the combined $u_r(k)$ is reduced to 0.56×10^{-6} . Assuming minimum correlations, $(k_{\text{present}}/k - 1) = 0.10 \times 10^{-6}$ and the combined $u_r(k)$ is reduced to 0.48×10^{-6} .

Keywords:

Boltzmann constant, acoustic resonance, microwave resonance, quasi-sphere, triaxial ellipsoid, speed of sound, definition of the kelvin

1. Introduction

Since 1968 the unit of thermodynamic temperature of the *Système International d'unités* (SI system) has been defined as $1/273.16$ of the temperature of the triple-point of pure water T_{TPW} [1]. International comparisons of triple-point of water cells show a dispersion of a few parts in 10^7 due mainly to variations in the isotopic composition of Standard Mean Ocean Water [2].

The need for ever increasing accuracy in temperature measurement has motivated the forthcoming new definition of the SI unit of temperature, the kelvin, based on a fixed value of the Boltzmann constant k [3]. Implementation is planned for 2018, concurrent with the re-definition of the SI base units, five of which, the metre, the ampere, the mole, the kilogram and the kelvin, will be based on fixed values of fundamental constants (respectively the speed of light *in vacuo*, the fundamental charge e , the Avogadro constant N_A , the Planck constant h and the Boltzmann constant k) [4].

Work has been underway in our laboratory and several other groups worldwide to make the most accurate determination of k possible before its value is fixed. Measurement techniques such as acoustic gas thermometry (AGT)[5] and dielectric-constant gas thermometry(DCGT)[6] have delivered the most accurate determinations of k , with relative uncertainties lower than 2 parts in 10^6 . We have opted for acoustic thermometry, which, strictly, measures the molar gas constant $R=kN_A$. However, since the relative uncertainty in the Avogadro constant, around 1.2×10^{-8} [7], is over an order of magnitude smaller than that of the most accurate measurements of R , the relative uncertainties in R and k are nearly identical.

We have already performed three determinations of k by acoustic gas thermometry in a 0.5 l resonator, one with argon [8] and two with helium-4 [9,10]. In this paper, we report on a new determination of k at the temperature of the triple point of water, using acoustic thermometry of helium-4 gas in a 3 l quasi-sphere.

The principle of the experiment is as follows. A gas-filled quasi-spherical resonator (QSR) is maintained in a thermostat at a known temperature (here $T_{\text{TPW}}=273.16\text{K}$ or within a few millikelvin of it, with measurements corrected for the small difference by a temperature ratio, other terms being sufficiently constant at the required level of accuracy). Acoustic resonance measurements are performed at different pressures of helium gas while the radii of the QSR are measured using microwave resonance. Great care is taken to avoid impurities in the test gas: a gas purifying system supplies a continuous flow of pure helium to the resonator to remove outgassing impurities. The amount of the only impurity that cannot be removed by purification, ^3He , is determined by mass spectrometry of samples from the same bottle as that used for the experiment.

In the following sections, we describe acoustic and microwave frequency measurements along three separate isotherms, two with a sound absorption lining in the thermostat, a third with it removed. The ensemble of data from the three runs is used to provide a value for the Boltzmann constant. We obtain $R=8.3144614(50)\text{ J}\cdot\text{mol}^{-1}\cdot\text{K}^{-1}$, yielding $k=1.38064878(83) \times 10^{-23}\text{ J}\cdot\text{K}^{-1}$ that is, a relative uncertainty $u(k)/k=0.60 \times 10^{-6}$, where the uncertainty is one standard uncertainty corresponding to a 68 % confidence level. The uncertainty budget for the present determination of k is reported in Table 1 where each line refers to a given section of the paper containing detailed information.

Table 1. Summarized uncertainty budget for the determination of the Boltzmann constant. Extensive details of how each component was obtained are given in the relevant sections.

Term	Effect on k (Parts in 10^6)	Section
Temperature measurements	0.39	4
Molar mass and gas purity	0.09	5
Volume measurements	0.20	6
Acoustic measurements	0.40	7
Total	0.60	Square root of the sum of squares

2 Principle of the experiment

The aim of the experiment is to measure the value of the Universal gas constant R . AGT is based on the measurement of the speed of sound c in a gas of known composition and therefore molar mass M in a resonator of known dimensions [5,11]. In an ideal monatomic gas, the squared speed of sound is given by:

$$c^2 = \frac{5}{3} \frac{RT}{M} = A_0, \quad (1a)$$

where T is the thermodynamic temperature. In a real gas, collisions between molecules and the resonator wall, the non-zero molecular volume and intermolecular interactions lead to pressure-dependent corrections to the squared speed of sound:

$$c^2 = \frac{A_{-1}}{p} + A_0 + A_1 p + A_2 p^2, \quad (1b)$$

where p is the pressure, and A_1 and A_2 the acoustic virial coefficients. The term A_{-1} is a semi-empirical coefficient. Higher-order corrections are possible but not considered here because, due to the limited pressure range of this experiment (≤ 700 kPa), the truncation error of the series expansion (1b) amounts to less than 0.01 parts in 10^6 .

The molar mass M of the gas must be accurately determined, implying that composition, impurity content and isotopic composition must be known. Among monoatomic gases, isotopic abundance considerations favour argon and helium-4. The former is composed of 99.6 % ^{40}Ar while ^4He samples contain only trace amounts ($\approx 10^{-6}$ or less) of ^3He .

The experiment presented in this paper is performed with ^4He , which has three advantages over argon. First, its thermophysical properties can be calculated *ab initio* with high accuracy. Secondly, provided impurities have been removed and there are no air leaks, the isotopic ratio is easier to determine and the relative amount of ^3He far lower than that of ^{36}Ar in natural argon. Thirdly, the resonance frequencies are higher by a factor $(M_{\text{Ar}}/M_{\text{He}})^{1/2} \approx \sqrt{10}$ than for argon gas in the same resonator. This means the modes studied are less likely to excite shell vibrations that perturb acoustic measurements.

The reader should bear in mind that, prior to starting the measurements with ^4He presented in this paper, we performed measurements in argon with the same apparatus. However, no accurate

determination of k was ever achieved because the scatter of measurements was unacceptably high, *i.e.* 20 times greater than in the present work. We discovered only recently that the cause was metallic swarf in the inlet and outlet tubes (used for gas flow), produced by diamond turning of the copper hemispheres with the tubes attached. The swarf randomly changed the acoustic impedance of the system, the effect of which was to increase the dispersion of the acoustic measurements. The obstructed ducts were subsequently removed and replaced, after which accurate measurements with argon would have been possible. However, time limits constrained us to restrict the work to helium.

In the case of helium, it is possible to make *ab initio* calculations of the coefficients A_i ($i= 1, 2$) to a level of accuracy comparable with or better than that available by experiment [12,13]. In our analysis, we use these *ab initio* values and set the term A_0 equal to $A_{0,CODATA} = (5/3) \cdot (R_{CODATA} \cdot T_{TPW} / M)$, R_{CODATA} being the 2014 CODATA value of the universal gas constant R [7]. This leads to a first approximation of the expected square speed of sound

$$c_{ab\ initio}^2 = A_{0,CODATA} + A_{1,ab\ initio} \cdot p + A_{2,ab\ initio} \cdot p^2. \quad (1c)$$

In our previous experiments, fits were made to squares of experimental sound velocities c_{exp}^2 as a function of p , and the pressure-independent part A_0 extracted. Given the now excellent reliability of *ab initio* calculations of the coefficients A_1 and A_2 , we fit the difference

$$c_{exp}^2 - c_{ab\ initio}^2 = \frac{A_{-1}}{p} + A'_0 + A'_1 p \quad (2)$$

where $A'_0 = A_0 - A_{0,CODATA}$ and $A'_1 = A_1 - A_{1,ab\ initio}$. To simplify the model we assume $A_2 \approx A_{2,ab\ initio}$. While the maximum value of the term $A_2 p^2$ corresponds, at 273.16 K, to less than 4×10^{-6} of the squared speed of sound, the use of this approximation introduces an additional uncertainty contribution quantified in Table 6 (uncertainty of *ab initio* speed of sound). The frequencies needed to calculate c_{exp}^2 before fitting with equation (2) are first corrected to take into account several perturbing effects, including shell motion, microphone effects and any unsuspected perturbations. We fit experimental speeds of sound to this model to determine the values of A_{-1} , A'_0 and A'_1 .

Practical measurements involve either acoustic velocity determinations at several different pressures to extract the pressure-independent term A'_0 [5,10] or else measurement at a fixed pressure and correction for its effect [14,15]. In our work, we use the former approach.

The remainder of the paper addresses the details of the measurement and is structured as follows. In section 3 we describe the principle of the experiment and the thermostat. Thereafter, in section 4, we outline the thermometry and pressure measurements. The issue of molar mass is presented in section 5 and the determination of the sphere radius in section 6. The acoustic measurements are described in section 7 and the overall uncertainty budget in section 8. Section 9 contains a summary and conclusions. Appendix A gives fitted parameters pertaining to three different methods of analysis of the acoustic data. Appendix B deals with correlated uncertainties between the four determinations of the Boltzmann constant at LNE.

3 Apparatus

The apparatus is adapted from that used in our previous measurement with helium [10]. The main difference is the use of a larger resonator. The 3 I QSR and the associated isentropic thermostat have been described briefly elsewhere [16]. We recall here that the resonator is a tri-axial ellipsoid made of high conductivity copper (CUA1). It is composed of two assembled hemispheres having a total mass of 14 kg. (For brevity, we use the term 'hemisphere' to refer to 'quasi-hemisphere'). The inner surfaces of the upper and lower hemispheres are diamond turned. The radii of the axes of the ellipsoid, determined prior to assembly using a coordinate measuring machine (CMM), are 90.074 mm,

90.134 mm and 90.174 mm. Loop antennae are used thereafter for real-time dimensional measurements via microwave measurements. Two acoustic transducers flush with the inner surface are used for emission and detection. The thermostat has a time constant of 6 h. The temperature of the heat shield is controlled to within $\pm 10\mu\text{K}$ and the set point is chosen such that there is no need to heat either the pressure vessel or the resonator. The only heat sources are thermometers generating around $100\mu\text{W}$ by their self-heating, and microwave absorption in the copper, adding another $200\mu\text{W}$.

4. Thermometry, gas handling and pressure measurements

4.1 Thermometry

The temperature of the resonator is measured using four Capsule-type Standard Platinum Resistance Thermometers (CSPRTs) (Tinsley⁹ 229073 and 203288, Hart Scientific⁹ HS135, Leeds & Northrup⁹ 1825277), two on each hemisphere. As in our previous work [8], we have used CSPRTs from three different manufacturers, all calibrated at the triple point of water using the same bridge, cables and standard resistance as those used in the determination of the Boltzmann constant.

CSPRTs provide the traceability to the temperature of the water triple point. The temperature of the resonator T_{res} is never centred exactly on 273.16 K, since this would lengthen the time of the experiment several-fold, which is unacceptable. The typical temperature deviations ΔT_{res} lie within $\pm 10\text{mK}$ from T_{TPW} and are evaluated from the average of the temperature measurements performed with the CSPRTs. They can be easily corrected in the data analysis, to yield speed of sound values at the temperature $T_{\text{TPW}} = T_{\text{res}} - \Delta T_{\text{res}}$. Since the sensitivity of each thermometer is accurately determined from its calibration, the uncertainty introduced by the offset correction never exceeds $10\mu\text{K}$.

We determined the homogeneity of the temperature across the resonator in the course of some of the experimental runs described in section 7.3. In particular, we measured the temperature homogeneity during run 1 at a pressure of 0.1 MPa, with a deviation from the water triple point temperature of $\Delta T_{\text{res}, 0.1\text{MPa}} = 6.04\text{ mK}$. Then we performed a second measurement during run 2 at 0.42 MPa, with $\Delta T_{\text{res}, 0.42\text{MPa}} = 9.01\text{ mK}$. Finally, we measured the homogeneity during run 3 at 0.65 MPa, with $\Delta T_{\text{res}, 0.65\text{MPa}} = 0.15\text{ mK}$. CSPRTs n 229073, 203288 and HS135 provided temperature measurements reproducible within 0.06 mK, comparable with their calibration uncertainties. On the other hand, the reproducibility of CSPRT n1825277 was 0.68 mK, seven times larger than its calibration uncertainty. We considered this thermometer to be unstable and so did not use its measurements to determine the thermal homogeneity of the resonator, nor to measure its temperature. Figure 1 shows the results of temperature homogeneity measurements performed with the three stable thermometers.

We attribute an uncertainty related to the homogeneity of 0.31 parts in 10^6 . Note that acoustic thermometry averages the thermal inhomogeneity [17]. Combined with the CSPRT calibration uncertainty, this yields an overall temperature uncertainty of 0.39 parts in 10^6 (see table 2).

⁹ In order to describe materials and procedures adequately, it is occasionally necessary to identify commercial products by manufacturers' name or label. In no instance does such identification imply endorsement by LCM-LNE, INRiM, or NIST, nor does it imply that the particular product or equipment is necessarily the best available for the purpose.

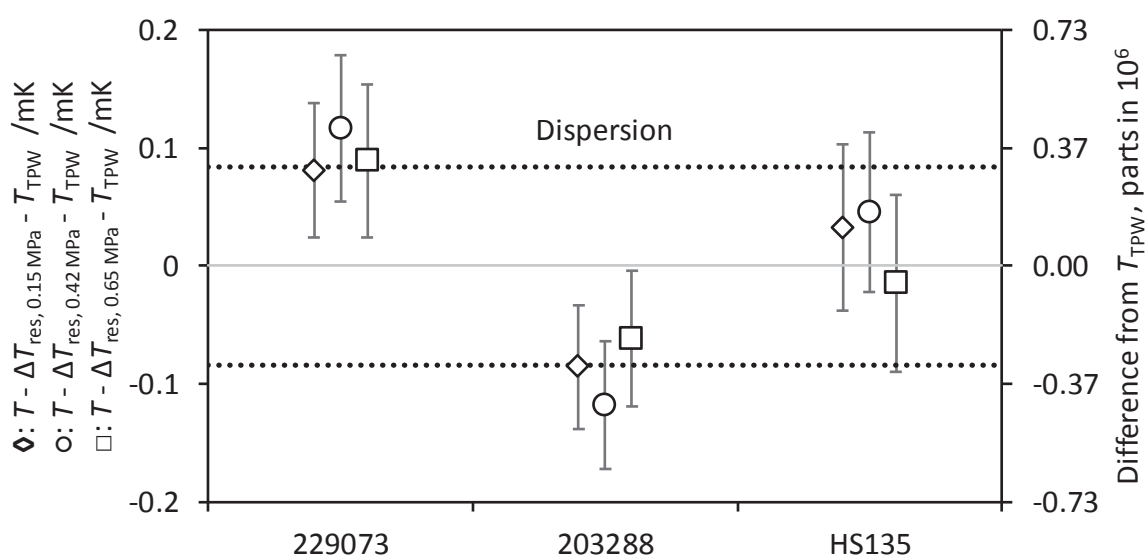


Figure 1. Temperature of the resonator measured using three different capsule-type standard platinum resistance thermometers, during three different runs at three different gas pressures. Values are expressed as differences with respect to T_{TPW} , both in millikelvin and in parts in 10^6 . The dotted lines represent the uncertainty interval related to the dispersion of thermometer readings.

Table 2. Uncertainty budget for the thermometry measurements for the determination of the Boltzmann constant at the triple point of water TPW. The dominant contribution arises from the dispersion of thermometer readings at different locations.

Term	Uncertainty in k (Parts in 10^6)	Note
Repeatability and self-heating	0.08	Evaluated with measurements performed on the resonator
Standard resistor stability	0.05	Temperature stability and time-drift of the standard resistor
Resistance bridge	0.04	Bridge linearity and bandwidth
Dispersion of thermometer readings	0.31	Standard deviation of the temperatures measured on the resonator (scaled to T_{TPW}), includes the contribution of the correction ΔT_{res}
TPW calibration	0.21	Calibration at the TPW, including TPW repeatability, isotopic effect, purity, hydrostatic head effect and heat fluxes
TOTAL	0.3	Square root of the sum of squares

4.2 Gas handling

The gas handling system is similar to that described in our previous measurement of the Boltzmann constant with helium ([10], figure 7). The main difference is that in this work only a single liquid-helium-cooled cold trap was used; it was maintained at 4.3K, and its volume was 4 cm³. (In previous work [10], another cold trap containing active charcoal was also employed). Ideally, the only impurity present after the cold trap should be trace amounts of ³He, all other gases being condensed.

As stated in section 2, the gas handling system and apparatus had previously been filled with argon which, for work with helium, had to be flushed out. Thus, a possible systematic error - related to residual amounts of argon remaining in the system downstream from the cold trap - might be suspected. Preliminary measurements of the speed of sound in helium were performed repeatedly for one month after the change of gas until a stable value was obtained. This was interpreted as indicating there was no more argon. One might suspect that if there were any argon in unseen cracks in the sphere surface, the amount of it would vary with the helium flow rate. Now the flow rate changes by more than a factor of three between the lowest (0.15 MPa) and highest pressure (0.7 MPa) yet no modification of the speed of sound was observed at the level of experimental resolution. It is assumed therefore that the appropriate molar mass for the determination of the Boltzmann constant is that of the gas supplied by the bottle. This was determined by mass spectrometry discussed below in section 5.

4.3 Pressure measurements

In the gas handling system, which has the same arrangement as that of our previous measurement with helium in the 0.5 l QSR [10], the pressure of the helium is both controlled and measured at the inlet of the QSR. The control is performed by a servo loop using a Paroscientific Inc. Digiquartz model 745 High Accuracy Pressure Standard⁹ gauge. The measurement is performed using an absolute pressure piston gauge. To minimise pressure corrections due to flowing gas, a line with a large impedance is installed between the inlet of the QSR and the control pressure gauge, while the impedance is about 62 times smaller between the QSR inlet and the piston balance. Aside from its accuracy, the piston gauge has the advantage that its calibration uncertainty is of the form $a + b \cdot p$. This implies that, in the extrapolation of the square speed of sound versus pressure, the linear component of the calibration uncertainty has no effect. In fact, the linear calibration term $b \cdot p$ affects the fitted semi-empirical coefficient A_1' , but has no impact on the measured value of R , since the latter is obtained from the coefficient A_0' .

The piston gauge used in this work (Ruska 2465-727⁹, piston-cylinder serial number C662) was calibrated by the Mass and Derived Quantities group at LNE. It delivered an uncertainty in pressure measurements $u_p = 0.14 \text{ Pa} + 7.0 \times 10^{-6} \times p$, yielding 5.1 Pa at the maximum pressure of 0.7 MPa used in this experiment. Such an uncertainty affects our determination of R by 0.05 parts in 10⁶.

Note that the piston gauge was unavailable for the four measurements performed in run 3. In that case, data from the control gauge were used to measure pressure. The control gauge was calibrated with an uncertainty of 7.5 Pa, but showed a hysteresis of 11.2 Pa. To be conservative, we decided to take this last value as the maximum estimate of our pressure uncertainty, which yielded a relative uncertainty in R of 0.1 parts in 10⁶ (table 6).

5. Molar mass

The possibility of a more accurate estimate of the molar mass is one of the major advantages of helium as the acoustic gas. In our experiment, we used ultra-pure helium at 99.9999% (Air Liquide Alphagaz 2⁹). Using a cold trap at 4.3K, all gases except ⁴He and trace amounts of ³He were removed. The trace amounts of ³He present in the ⁴He were determined at the *Centre de Recherches pétrographiques et Géochimiques* (CRPG). In addition, we performed experiments to assess the absence of any other significant gaseous impurity inside the resonator. Table 3 summarizes the uncertainties related to the determination of the molar mass of helium. Details are given in sections 5.1 and 5.2.

Table 5.1 Uncertainty budget for molar mass determination. The relative change in the molar mass gives an identical relative change of the Boltzmann constant k .

Term	Effect on k (Parts in 10 ⁶)	Note
³ He/ ⁴ He ratio	0.01	Uncertainty estimate from CRPG-CNRS (section 5.1)
Impurity	0.02	Change of two bottles (section 5.2)
Estimated outgassing	0.08	Effect of gas flow change (section 5.3)
Single cold trap effectiveness	0.03	Supplementary study using Ar seeded He gas. (section 5.4)
Difference of two cold traps	0.03	With or without charcoal [10]
Total	0.09	Square root of the sum of squares

The following sub-sections explain how the uncertainties in Table 3 were determined.

5.1 Determination of ³He content in ⁴He

Gas samples were collected from the inlet tube of the resonator in two different conditions, namely with or without the liquid helium cold trap. The reason for this was to see whether the presence of impurities would have any effect on the measured ³He/⁴He ratio. The samples were then sent to CRPG for the analysis of their ³He content. Details of the experimental set-up available at CRPG are given in Mabry *et al.* 2013 [18] and 2015 [19]. The system uses a Thermo Scientific Helix Split Flight Tube Noble gas mass spectrometer⁹. The instrument, specifically designed for helium isotope analysis, incorporates a split flight tube that physically separates the beams of ³He and ⁴He ions. The spectrometer has a resolving power ($M/\Delta M$) of 700, large enough to separate the ³He peak from those of its isobars tritium (³T) and hydrogen deuteride (HD). The ions are detected using a Faraday cup of resolution 425. Stray ions are removed by an electrostatic filter located before the multiplier. Helium mass spectra are obtained at a trap current of 400 μ A with an accelerating voltage of 4.5kV. Under these conditions, the helium sensitivity is 2.35×10^{-4} A·torr⁻¹. To minimize perturbations due to HD, an SAES getter⁹ is installed on the mass spectrometer to absorb all molecular isotopes of hydrogen. The background of argon and other heavier isotopes is kept low with the help of a liquid-helium-cooled trap maintained at around 25 K with a temperature stability of ± 50 μ K.

The measurements on our gas samples were carried out in two steps: purification, then mass spectrometry. To perform the purification, the gas was handled in a high-vacuum line (the pressure being in the range 10^{-6} Pa). An aliquot of the gas of interest was purified and equilibrated in a trap containing charcoal held at liquid nitrogen temperature (≈ 77 K) for 20 min, to remove all species but neon, helium and hydrogen. The remaining gas was then expanded in another part of the line where it was sequentially trapped for 10 min in each of a suite of two getters held at 400 °C and room temperature, respectively, and another charcoal trap at liquid nitrogen temperature.

After purification, helium and neon were trapped in a cold head containing a few grains of charcoal held at 10 K. The temperature was then raised to 45 K to release helium, which was then analyzed isotopically. After analysis of the helium, the cold head temperature was raised at 105 K to release neon, which was then analyzed for its abundance in the same mass spectrometer. The instrument was calibrated daily with aliquots of a standard gas containing atmospheric helium and neon [19]. For atmospheric air, the helium-to-neon ratio should lie close to 0.3 whereas it should be infinite for a bottle of pure helium. The ratio is thus an indicator of any air contamination. We found a value $^4\text{He}/\text{Ne} > 2000$, strongly suggesting there was no air leak in the system.

From the analysis of the two gas samples sent to CRPG, we find ratios $^3\text{He}/^4\text{He}$ of 4.42×10^{-8} (with no cold trap) and 3.55×10^{-8} (with a cold trap). Though smaller than in [15,20], these ratios are compatible with the isotopic ratio $^3\text{He}/^4\text{He}$ of natural gases, from which industrial helium is extracted. Such a ratio varies generally over two orders of magnitude, from 10^{-8} for the pure radiogenic end-members to 10^{-6} for gases having incorporated a significant mantle-derived component [21]. Thus, each gas reservoir has its characteristic He isotope signature, depending on its tectonic context.

The presence of helium-3 at a level of a few parts in 10^8 reduces the value of the Boltzmann constant by 0.01 parts in 10^6 with respect to a gas of pure helium-4.

5.2 Gas Impurity estimation by change of gas bottle

To evaluate the effect of the residual impurities in the gas, we performed three experiments. The first was a change of the gas cylinder supplying helium to our apparatus, with another bottle of the same nominal purity. The objective was to check the effectiveness of our purification system, composed of a getter and a liquid-helium cold-trap [10]. The effect of changing the bottle was investigated using the acoustic resonance frequencies. The difference in results obtained using one or other of the bottles (0.03 parts in 10^6 in the value of c^2) was indistinguishable at the noise level of the experiment even after eight times the recycling time needed to refresh all the volume in the sphere. This compares with our previous measurement with helium [10] where the change was +0.5 parts in 10^6 . In retrospect, we suspect there was problem with the cold trap used at the time, *i.e.* too low a level of liquid helium in the Dewar. The test of cold trap efficiency described below has boosted our confidence in that assertion.

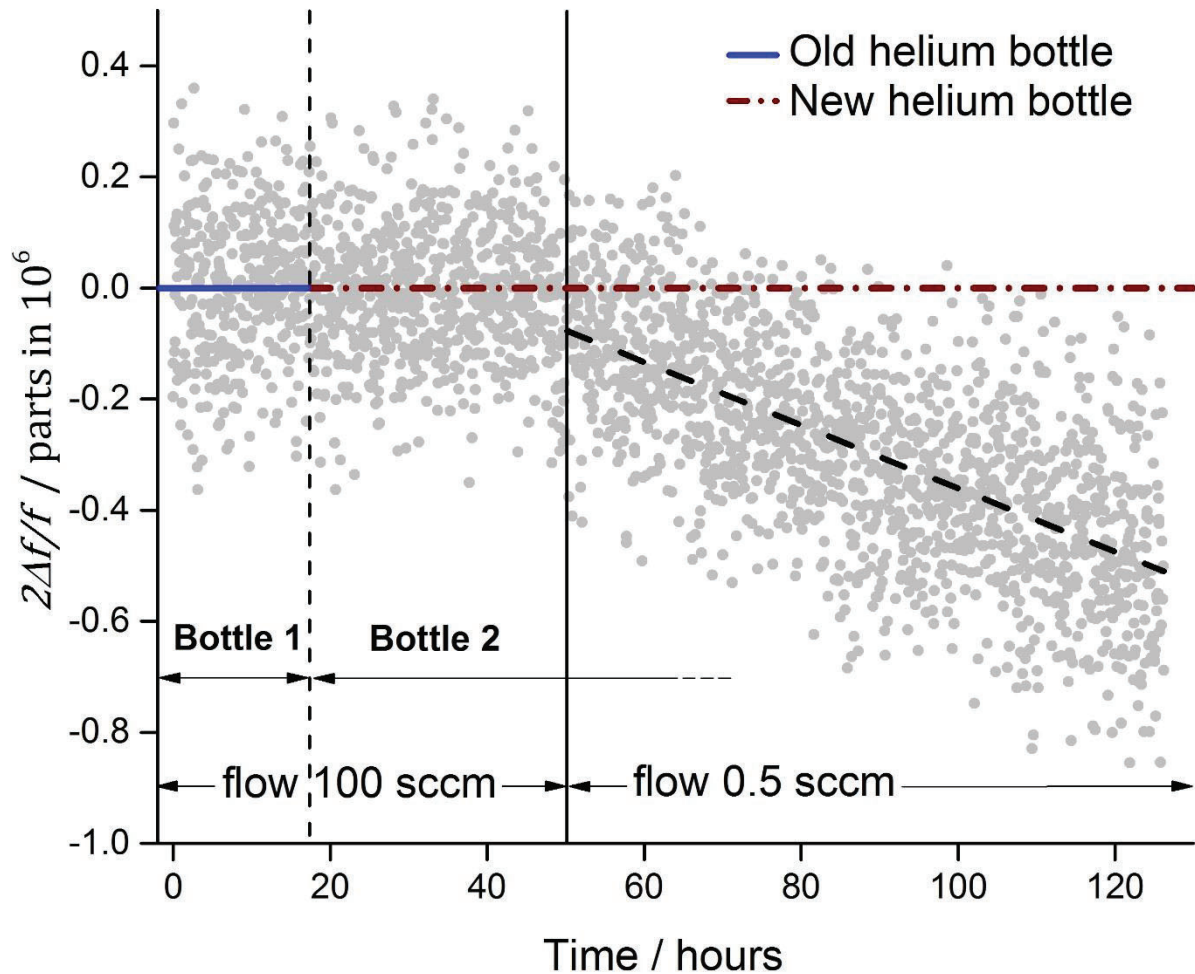


Figure 2. Effects of changing helium bottles and flow rate. The vertical axis displays double the relative frequency variation $2\Delta f/f$ for the mode (0,3). For the first 18 hours, the original bottle was used, after which it was changed. Any change in the resonance frequency is imperceptible. After 50 hours, the gas flow was throttled down to the minimum rate. The effect of outgassing of the resonator is manifest, producing the negative slope.

5.3 Estimation of outgassing

The second test for the evaluation of impurity effect was a gas flow change at a pressure of 0.65MPa. The gas flow was lowered by a factor around 100 to make visible the effects of the impurities outgassing from the resonator bulk. (It was not shut off completely so we could still control the pressure by a servo loop. A shut valve and closed volume would have led to pressure fluctuations related to those of the ambient temperature). Initially we recorded the frequency of the acoustic mode (0,3) at a constant flow rate of 100sccm¹⁰; thereafter we reduced the flow rate to a mere 0.5 sccm¹⁰ and measured the progressive negative drift of the frequency over the next 70 hours (Figure 2). A linear fit to the data gives an estimate of $-0.0054 \text{ ppm h}^{-1}$. Assuming this variation is caused by outgassing of water from the inner surface of the resonator, we calculate the corresponding outgassing rate of $8 \times 10^{-12} \text{ mol} \cdot \text{m}^{-2} \cdot \text{s}^{-1}$, which is compatible with typical rates for metal surfaces after prolonged evacuation. As in [14], we use this estimate to calculate the maximum possible concentration of water

¹⁰sccm = standard cubic centimetres per minute, corresponding to $1.6667 \times 10^{-8} \text{ m}^3 \cdot \text{s}^{-1}$ in the International System of Units (SI). We define the volumetric flow 1 sccm as the flow of 1 cubic centimetre per minute of argon at a pressure of 103 kPa and temperature of 20 °C.

vapour in the working gas under normal experimental conditions, *i.e.* with helium flowing at 100 sccm, with the result $x_{\text{water}} = 0.008$ parts in 10^6 and a possible corresponding effect on our estimate of M of -0.03 parts in 10^6 . If our assumption that the observed drift of the mode (0,3) frequency being due to outgassing of water vapour were wrong, and the cause was instead a virtual leak of argon from a small volume communicating with the resonator with a large impedance to flow, then the concentration of argon in our working gas would be $x_{\text{Ar}} = 0.008$ parts in 10^6 and the possible corresponding effect on our estimate of M of -0.07 parts in 10^6 . All things considered, we ascribe an uncertainty to our estimate of impurity for M of 0.08 parts in 10^6 (Table 3).

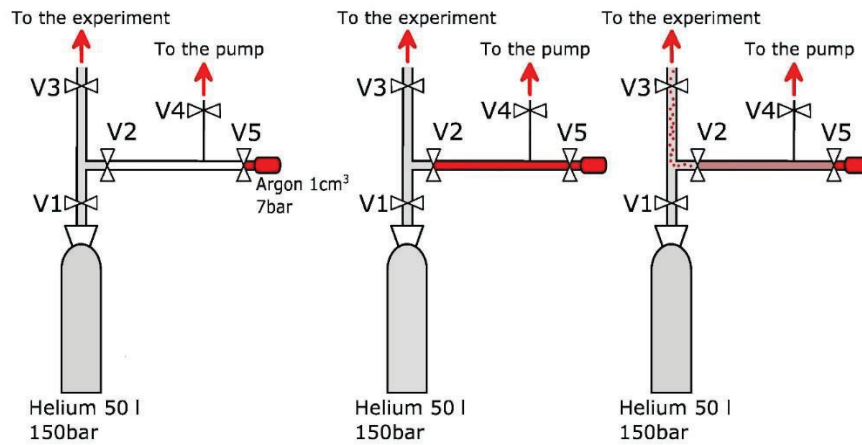


Figure 3. Gas handling in a complementary study to demonstrate the effectiveness of a liquid helium cooled trap in removing argon gas. Left: A small volume was filled with natural argon and attached to the end of a long thin tube (3mm diameter, length 1m) via a valve (V5). The tube is pumped out to a few pascals. Middle: Valve V5 is opened and becomes filled with argon. Right: Valve V2 is opened to mix the argon and helium gases in the long tube; argon diffuses into the helium flow bound for the acoustic resonator.

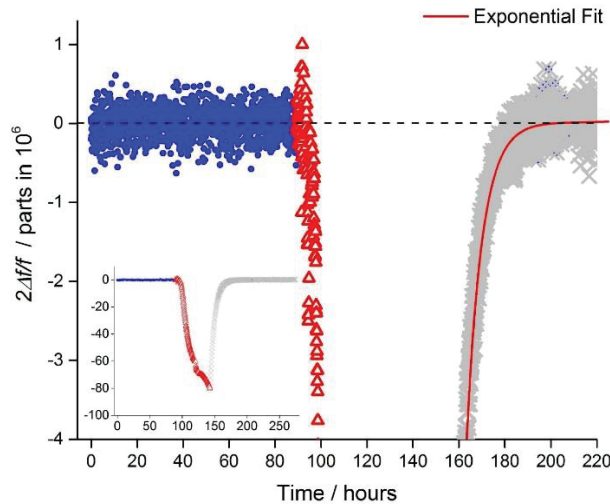


Figure 4. Measurement of the effectiveness of a liquid-helium-cooled trap to remove argon gas. The square of the speed of sound is proportional to the square of the frequency of a give acoustic mode. Here we use the mode (0,3) at 0.625MPa. Left (blue): Normal conditions, flowing helium-4 purified by the cold trap. Middle (red): cold trap by-passed with diffusion of argon as described in Figure 3. The frequency shift of ≈ 85 parts in 10^6 is manifest. Right (grey): re-introduction of the cold trap.

5.4 Cold trap effectiveness

Following the present campaign of measurements, a third, supplementary experiment was performed to demonstrate the effectiveness of the cold trap (Figures 3 and 4). To simulate the effect of contamination in the bottle, we prepared a mixture in an evacuated one metre long tube into which a small amount of argon gas was introduced before the rest was filled with pure helium ahead. Due to the diffusion, the molar concentration of natural argon rose gradually to 9.5 parts in 10^6 , following an error function shape in accordance with the theory of diffusion. In a first instance, acoustic measurements with no cold trap showed an 85 parts in 10^6 decrease of the speed of sound squared compared with pure helium.

The cold trap was then re-installed and, as expected, the shift diminished exponentially as the argon was removed (Figure 4). The amount of argon diminished following the exponential law $(1 - \exp(-t/\tau))$ with $\tau = 6.8\text{h}$. After 115h the relative frequency shift was 0.03 parts in 10^6 . Note that for the measurement of the Boltzmann constant, the cold trap is in place for typically 400 hours. After 48 hours, no shift was discernable at a level of 0.03 parts in 10^6 . We ascribed this value as an uncertainty component in k related to the effectiveness of the cold trap.

Because of time constraints, we did not introduce neon into the helium for the present demonstration (Fig. 4) of the effectiveness of the cold trap. However, in a previous publication [10], we compared the present cold trap (a simple cylinder of volume 4 cm^3 directly in contact with the liquid helium at 4 K) to a second cold trap, of volume 10 cm^3 and filled with charcoal that had a much larger surface at 4 K. Averaged over several hours, the square of the speed of sound in the helium gas delivered by the two cold traps differed by no more than 0.03 parts in 10^6 , demonstrating the equivalence of the two cold traps. Others have shown [22] that charcoal-filled cold traps reduced the neon concentration in helium to 2×10^{-9} , even when the traps were at much higher temperature, near 35 K. Finally, we note that Gavioso *et al.* [14] had three samples of commercially purified helium analyzed for neon; the largest mole fraction that they reported was $x_{\text{neon}} = (0.07 \pm 0.02) \mu\text{mol mol}^{-1}$.

6. Resonator dimensions

As briefly recalled in section 3, the acoustic resonator is a tri-axial ellipsoid composed of two diamond-turned hemispheres bolted together at the equator. Before the resonator was assembled, the radii of the three axes were measured using a CMM. After assembly, the radii were measured by microwave resonance measurements following the method described in many articles *e.g.* [8, 23]. The main idea is to measure the triplets of the TM_{1n} and TE_{1n} modes ($n = 1, 2, 3$ etc.), apply the corrections to account for holes and antennae [24], then calculate the second-order shape correction to deduce the radius [25,26]. Without the latter correction, it would not have been possible to obtain the very low uncertainty in earlier work [8-10,23] and here.

For the determination of k , the radii were determined constantly *in situ* by microwave measurement with both TE and TM modes (the latter being sensitive to surface quality). To provide redundancy, microwave frequency scans were performed over 10 different modes, TE_{11} to TE_{15} and TM_{11} to TM_{15} , to provide redundancy. The central frequencies yield the radii while the measured half-widths of the resonance are a measure of the quality factor of the system, itself a function of the surface conductivity. Since microwave scans are interspersed with acoustic frequency measurements, the gas pressure in the resonator can change from one microwave measurement to another. Microwave measurements are therefore corrected for the refractive index of helium, including the polarisability [27] and the second dielectric virial [28].

Results for measurements of mode frequencies and corresponding radii are shown in Figure 5. As in [10], the radius a corresponds to the *geometric* mean of a_x , a_y and a_z , i.e. $(a_x \times a_y \times a_z)^{1/3}$ while $\langle a \rangle$ is the average of this mean over all ten modes shown. A relative difference of 1×10^{-7} between the radius a derived from mode TM11 and the others was also observed in earlier work, a fact not too surprising since it is the mode most sensitive to surface effects such as imperfections caused by the insertion of acoustic transducers.

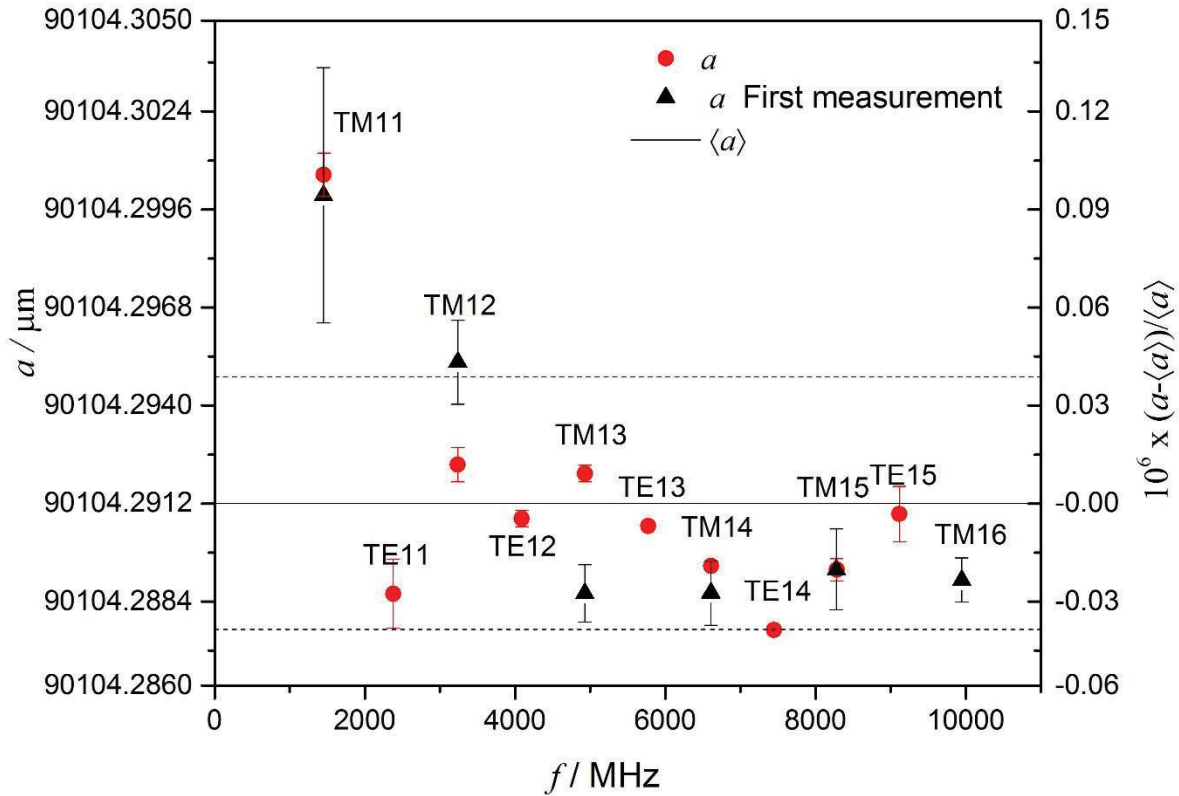


Figure 5. Measurements of mean spherical radius a corresponding to the modes TM11, TE11, TM12, TE12, TM13, TE13, TM14, TE14, TM15 and TE15 in order of ascending frequency. The solid line corresponds to the average radius $\langle a \rangle$ and the dotted lines the standard deviation. Values are referred to conditions of zero pressure and a thermodynamic temperature of 273.16 K. The triangles correspond to the values obtained by the very first measurements for which diamond-turned plugs flush with the inner surface were used instead of microphones. The circles give the values measured with the microphones in place.

We found good agreement between the ellipticities ε_1 and ε_2 [8] determined *in situ* and, less accurately, by the CMM (from the CMM $\varepsilon_1 = 0.1315 \times 10^{-2}$ $\varepsilon_2 = 0.705 \times 10^{-3}$ [29] and by microwave resonance $\varepsilon_1 = (0.13140 \pm 0.0001) \times 10^{-2}$ $\varepsilon_2 = (0.7021 \pm 0.001) \times 10^{-3}$ [25,26]). We also measured the radius as a function of the helium pressure (for all modes above) and thereby determined the compressibility of the copper used to make the resonator (Figure 6): the elastic compliance of the shell $k_T = (1/a)(\partial a / \partial p)$ with the result $k_T = -(7.580 \pm 0.026) \times 10^{-12} \text{ Pa}^{-1}$. The thermal expansion of this resonator was obtained from the same microwave measurement. During the different measurements, all the data were taken at temperatures in the range of ± 20 mK around 273.16 K. This temperature dispersion was used to estimate the thermal expansion of the sphere via the radii obtained by microwave resonance. This gave a value for the linear coefficient of thermal expansion α_{th} of the cavity of $(1.584 \pm 0.006) \times 10^{-5} \text{ K}^{-1}$. Using the same method as previously [8], from the half-width of the TE11z mode, we obtained a value for the electrical resistivity of $1.59 \times 10^{-8} \Omega \cdot \text{m}$ at 273.16 K. Once again [8], using this value, we computed the half-widths of the other modes (Figure 7). We use the difference

of this estimated value and that measured over all the modes as a measure of the uncertainty for the electrical conductivity.

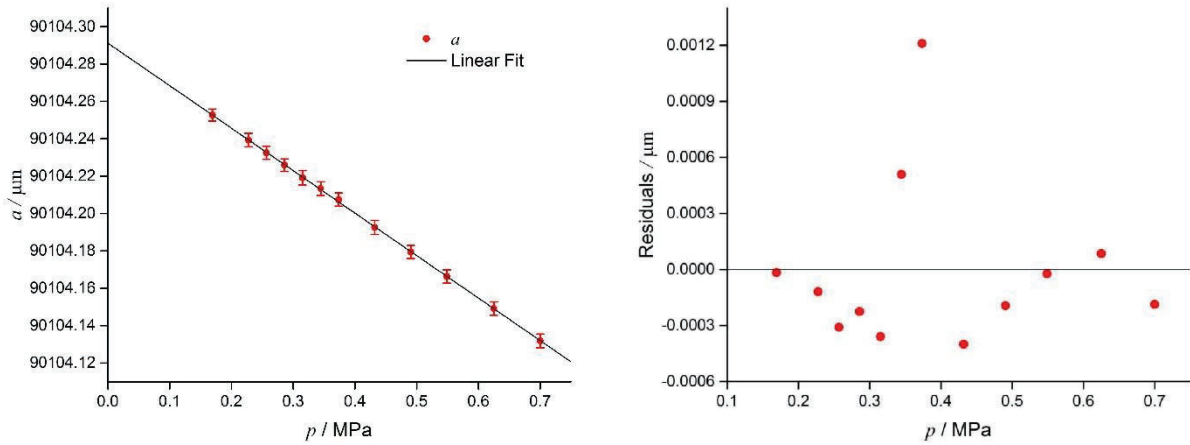


Figure 6 Left: Cavity radius a as a function of pressure p at 273.16 K. Right: Residuals from a linear fit. The line refers to data and residuals from the arithmetic mean of all modes. Microwave estimates of the resonator radius at zero pressure are obtained by extrapolating to zero pressure microwave data measured at different pressures along the isotherm. The two measurements at 0.7 and 0.37 MPa were made with a thermal stability drift of around $1\text{mK}\cdot\text{h}^{-1}$; for the other data, the drift was less than $0.1\text{mK}\cdot\text{h}^{-1}$. Note that the amplitude of the residuals corresponds to less than 10^{-8} of the radius, which is remarkable. Thanks to the use of piston balance, the relative uncertainty in the pressure was less than 7 parts in 10^6 .

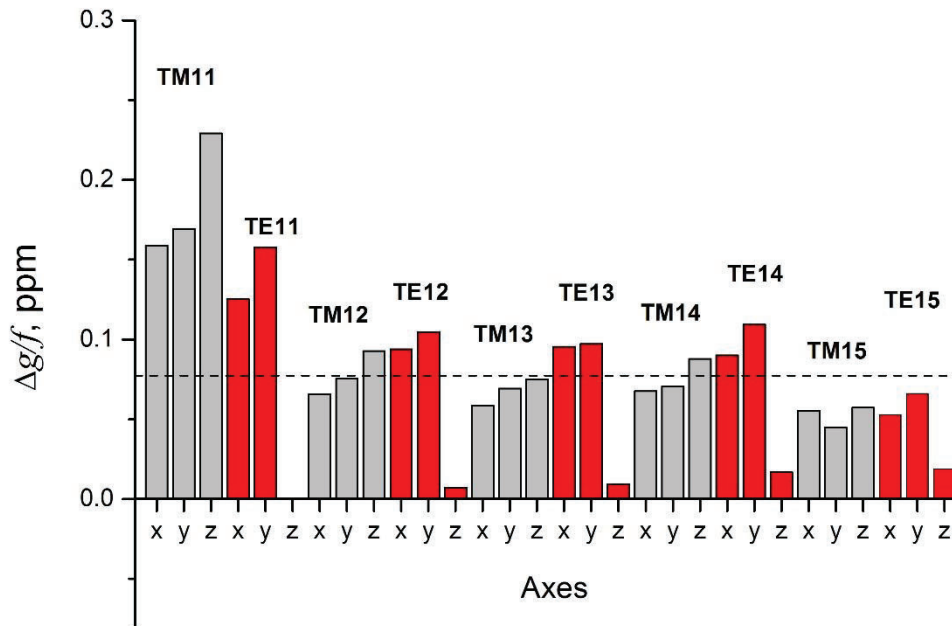


Figure 7 Relative excesses half-widths $\Delta g/f$ determined using the electrical resistivity deduced from the half-width of the microwave mode TE11z resonance.

The uncertainty budget for the microwave measurements is given in Table 4. The fitting uncertainty of microwave resonances is governed by the signal-to-noise ratio (SNR) (10^4) and quality factor (250000). The hertz-level resolution is roughly the linewidth of the resonance divided by the SNR. The microwave oscillator frequency, referenced to a rubidium clock, has an uncertainty that affects k below the level of 10^{-10} . The scatter between the ensemble of modes studied, shown in Figure 5, contributes a relative uncertainty of 0.08×10^{-6} . Temperature measurements affect the value of the

radii deduced via the thermal expansion coefficient of copper. The effect of temperature uncertainty on the value of the refractive index is negligible. The temperature uncertainty, discussed above in section 4, includes the calibration uncertainty of the thermometers and the temperature spread over the volume of the QSR. Each of these affects the value of k , via the dimensional measurement, at a level of 0.009×10^{-6} . Due to the finite surface conductivity of copper, dimensional measurement must be corrected for skin depth. Moreover, the spread in the values of this conductivity between modes leads to a relative uncertainty in k of 0.08×10^{-6} . Deviations from a perfect tri-axial ellipsoid are caused by the insertion of acoustic transducers and microwave antennae. These are referred to in Table 6.1 as the “microphone perturbations” (relative uncertainty in k of 0.023×10^{-6}) and “waveguide corrections” (relative uncertainty in k of 0.05×10^{-6}). The effect of transducers was estimated from the difference between the radius obtained with the TM11 mode during initial measurements (with no transducer) and later ones with transducer (figure 5). The effect of antennae shape was quantified as the difference in values of radii measured with either straight or loop antennae. Although the copper resonator was maintained under vacuum or inert gas, an inevitable oxide layer formed on its surface prior to this. The effect of this dielectric layer leads to a relative uncertainty in the value of k of 0.067×10^{-6} . Assuming all these contributions to be independent, we obtain from the square root of their quadratic sum, a relative uncertainty in k of 0.16×10^{-6} .

Table 4 Uncertainty budget for microwave determination of resonator dimensions. For detailed explanations of the components see Pitre *et al.* [8] which uses the same technique applied to a resonator of volume 0.5 l.

Uncertainty component	Effect on k in parts in 10^6	Note
Resonance fit	0.008	Fitting uncertainty
Extrapolation to zero pressure	0.008	Uncertainty intercept of extrapolation
Scatter among microwave radii (includes uncertainty of shape perturbation)	0.08	Agreement between the TE and TM modes
Frequency reference	0.0	< 1 part in 10^{10}
Temperature calibration	0.009	See Section 4 thermometry
Temperature gradient	0.009	See Section 4 thermometry. Dispersion lower than 0.09 mK
Surface conductivity	0.16	Scatter of the average conductivity relative to the conductivity obtained using the TE11z mode
Microphone perturbation	0.023	Shift between the radius obtained with the TM11 mode and that of the other modes at the time of the first measurement and currently.
Waveguide corrections	0.05	Difference between the radii observed with straight and loop antennae
Dielectric layer	0.067	Difference in the radii obtained with only TM modes and only TE modes
Total	0.20	Square root of the sum of squares

7. Measurement and analysis of acoustic resonance properties of the cavity

We recall the principle of the method used to measure the speed of sound via acoustic resonance frequencies [11] then describe how data are corrected to account for several physical effects. The equipment, instruments, sensors and techniques to measure the acoustic field in the resonator and detect resonance frequencies and half-widths are very similar to those used in our previous work [8,10,30]. Aside from the larger resonator volume, the main difference relates to the sound source and acoustic sensor which here are two identical ¼” condenser microphones (GRAS 40BF⁹) flush-mounted on the wall of the cavity. The corrections are all estimated using well-established models [5,8,11], [31-33].

7.1. General principle

The speed of sound $c(p,T)$ at a given pressure and temperature can be related to the acoustic resonance frequencies f_{0n} of the radial modes in an ideal gas-filled spherical cavity. For the type of quasi-spherical cavity considered here, and the radial acoustic mode of $(0,n)$, this relationship can be written as

$$c(p,T) = 2\pi a(p,T) \frac{f_{0n}^A(p,T)}{Z_{0n}^A}, \quad (3)$$

where $a(p,T)$ is the equivalent radius determined in section 6 and Z_{0n}^A the eigenvalue of the acoustic mode considered, close to the zeros of the first derivative of the corresponding spherical Bessel function and accounting for the real shape of the cavity [25,34].

We obtain the ideal resonance frequency f_{0n} by adding to the measured acoustic resonance frequency f_{0n} a correction term Δf_{0n} that includes all the perturbing acoustic effects occurring in the cavity (see section 6.3). These correction terms are calculated from analytical models of the acoustic field in the “perturbed” cavity [32,35]. The half-width g_{0n} associated with the acoustic mode can be predicted by the same models. The excess half-widths between measured and calculated values provide a check on the validity of these models.

To determine the values of f_{0n} and g_{0n} experimentally, we use the same frequency scanning scheme as in Pitre *et al* [8] (same number of points and same spacing). As there, only a linear background is used for the complex resonant function. The acoustic modes acquired here are the first eight radial modes, *i.e.* modes $(0,2)$ to $(0,9)$, at several pressures from about 0.14 MPa to 0.70 MPa, and at temperatures close to T_{TPW} (Isothermal).

7.2. Acoustic perturbations and correction terms

The speed-of-sound measurements are corrected for several physical effects, most significantly the thermal boundary layer. The other corrections are related to bulk dissipation, temperature discontinuity between the acoustic gas and resonator surface, duct effects of inlet and outlet tubes and the properties of the acoustic transducers. The thermal conductivity of the wall is neglected here (effect lower than 5×10^{-9}). After years of experimental and theoretical effort especially by the NIST group [5,11,35,36], but also elsewhere [31-33], all the corrections are considered to be well understood.

In this latest experiment, special attention was paid to the effect of the inlet and outlet gas ducts. The ducts, *i.e.* long, narrow cylindrical tubes flush-mounted on the wall of the cavity, induce acoustic perturbations whose effects are estimated using well-established models of acoustic plane-wave propagation in cylindrical open ducts [34,37,38]. Given the dimensions of the ducts, the influence of their terminal radiation impedance [39] is negligible. The length of the tube was chosen to minimize the acoustic effect. The inlet tubing is very long (6 m) to thermalise the gas and minimise perturbations to the acoustic frequency. By contrast the outlet tube is relatively short (8.77 cm) since the flowing gas pressure is measured on this side. The choice of length was somewhat critical and resulted from a compromise that would perturb least the ensemble of acoustic modes to be studied [29]. Both tubes have a radius of 0.507 mm. Following Gillis *et al* [38], to estimate the uncertainty due to the effect of the tube, we changed the radius by 10 %.

The perturbing effects of the acoustic transducers could be estimated using models of condenser microphones, [33,40,41]. However, to calculate correction terms one requires an accurate knowledge of the parameters of individual microphones which are not accessible to direct measurements, notably the tension of the membrane. For this reason, we include an extra term in the uncertainty budget (see section 7.4), which turns out to be one of the largest.

We have also taken account of the penetration of a thermal wave into the cavity wall. This effect is well modelled in the supplementary data A in [5]. Due to the large heat capacity of the copper resonator compared with that of the helium gas, this effect reduces the speed of sound by only 0.091 parts in 10^6 for all the modes.

In principle, the frequency dependence of the half-widths in the fitting function requires an additional correction to the fitted parameters f_{0n} and g_{0n} of the order $(g_{0n}/2f_{0n})^2$ [42]. In practice, the maximum relative value of this correction for mode (0,2) is 0.03 parts in 10^6 at 0.15 MPa, with a negligible impact on our final determination of the speed of sound at zero pressure.

Finally, the coupling between the acoustic field in the gas and the resonator shell can generate strong perturbations to acoustic modes whose frequencies lie close to vibration resonances of the shell [43]. If the prediction of these frequencies for a real resonator (sphere with equatorial rim, bolts and support) is an exceedingly difficult task, such a calculation is of great help for the design of the cavity since it provides an estimation of where the normal modes are likely to occur. On the other hand, it is not accurate enough to allow corrections to acoustic frequencies at the sub-part-per-million level required in the present experiment. Note however that the effect, which is approximately linear as a function of pressure, has no consequences on the zero-pressure extrapolation of the acoustic data and thus does not contribute any uncertainty to the determination of k .

To check for consistency, it is desirable to study as many acoustic modes as possible [5]. Here we excited modes (0,2) to (0,9); modes (0,7) and (0,9) were excluded from determinations of the speed of sound due to their large excess half-widths caused by overlap and/or coupling with other modes. An advantage of helium-4 over argon as far as shell vibrations are concerned is that corresponding acoustic mode eigenfrequencies are $(M_{Ar}/M_{4He})^{1/2} \approx \sqrt{10}$ times higher and so less likely to excite them. (With the present resonator filled with helium-4 we shall see that only modes (0,2) and possibly (0,3) are significantly perturbed by shell vibrations whereas with argon, four of them are (0,4), (0,5), (0,6) and (0,8)).

7.3. Isotherm analysis and fitting function for the speed of sound

As mentioned in the introduction (equation (2)), rather than fit square sound velocities to a pressure-dependent function and extract the zero-order term A'_0 to deduce the ideal gas limit of the speed of sound, we fit instead the difference between experimental values and *ab initio* predictions based on the CODATA 2014 value of A'_0 . Three runs were performed to obtain the data. In the first two, the inner wall of the pressure vessel was lined with cotton fabric to dampen any sound emitted by the sphere within it. For the third run, the fabric was removed. The residuals from a fit with equation (2) to the data for the radial mode (0,2) are shown in figure 8. Instead of decreasing with rising pressure, they fall then rise again at the highest pressure. This effect is much less apparent in the residuals for mode (0,3) whose frequency lies further away from that of a shell resonance (figure 9); indeed, it might be statistically absent. For the mode (0,4) whose frequency lies well away from any shell resonance, no pressure dependence is discernible (figure 10). The same is true for modes (0,5), (0,6) and (0,8). Consequently, mode (0,2) was not used to measure the Boltzmann constant. Figure 11 shows the excess half-widths scaled by $2 \times 10^6 f$ for the different modes. The fact they are all small indicates good agreement with the model. Figure 12 shows a plot of the function $\Delta g_{0n} / (g_{0n})$, which describes the increase of the half-widths at low pressure due to thermal boundary layer losses. The convergence of all the intercepts towards zero indicates the good quality of the acoustic model at low pressure. Figure 13 shows residuals of the fits of the pressure-dependent function of equation (2) to selected acoustic data for five radial modes in the pressure range 0.15 MPa-0.7 MPa. The error bars correspond to the type-A fitting uncertainty of each single datum shown in figures 8, 9 and 10. The residuals obtained using the three different fitting methods described below are identical to the naked eye.

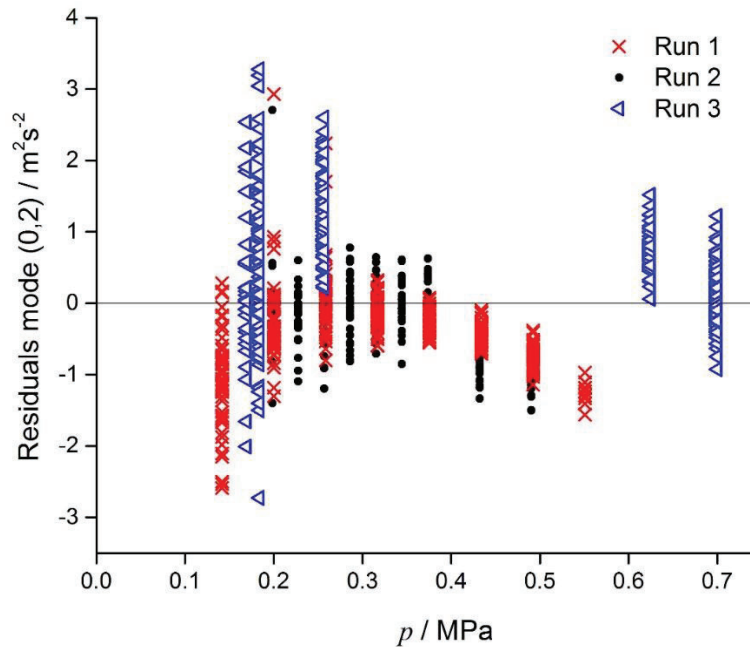


Figure 8. Residuals of fits of the difference of experimental and *ab initio* square sound speeds as a function of pressure for the radial acoustic mode (0,2) studied during three separate runs. The greater dispersion at lower pressures results from the lower signal-to-noise ratio. The marked difference at low pressures between runs 1 and 2 (acoustically damped pressure vessel) and run 3 (undamped) strongly suggests a shell vibration related effect. The noise in run 3 is higher for some inexplicable reason. None of the other modes exhibit this behaviour.

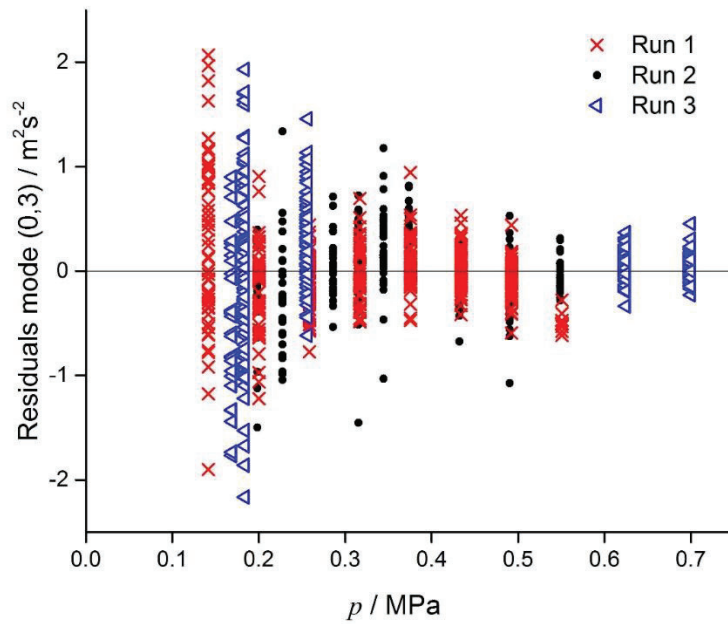


Figure 9. Residuals of fits of the difference of experimental and *ab initio* square sound speeds as a function of pressure for the radial acoustic mode (0,3) studied during three separate runs. The greater dispersion at lower pressures results from the lower SNR. The difference at low pressures between run 3 and runs 1 and 2 at low pressures hints at a shell vibration related effect.

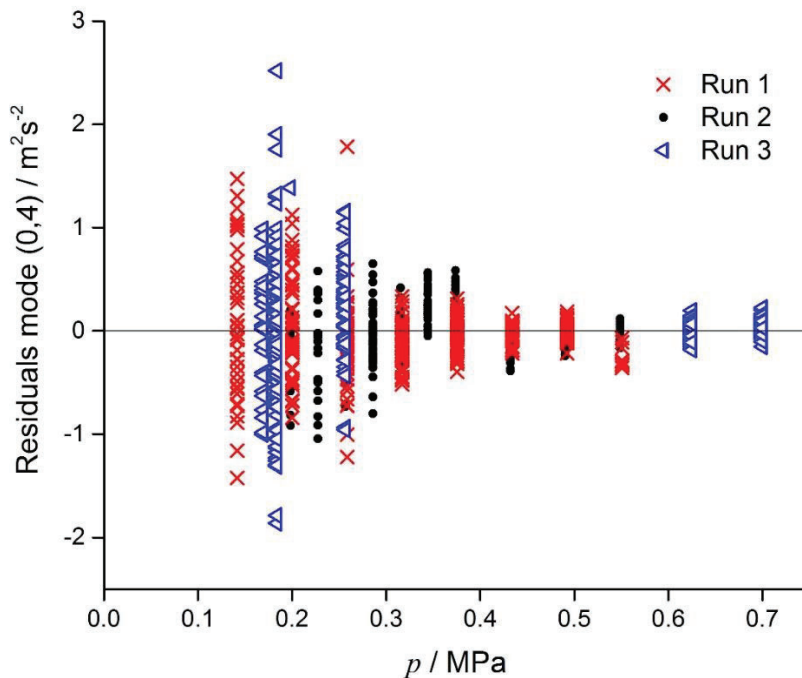


Figure 10. Residuals of fits of the difference of experimental and *ab initio* square sound speeds as a function of pressure for the radial acoustic mode (0,4) studied during three separate runs. The greater dispersion at lower pressures results from the lower SNR. Unlike the case of modes (0,2) (figure 8) and (0,3) (figure 9), there is no obvious difference at any pressure between runs 1 and 2 (acoustically damped pressure vessel) and run 3 (undamped) since the frequency of mode (0,4) lies far from any shell vibration resonance.

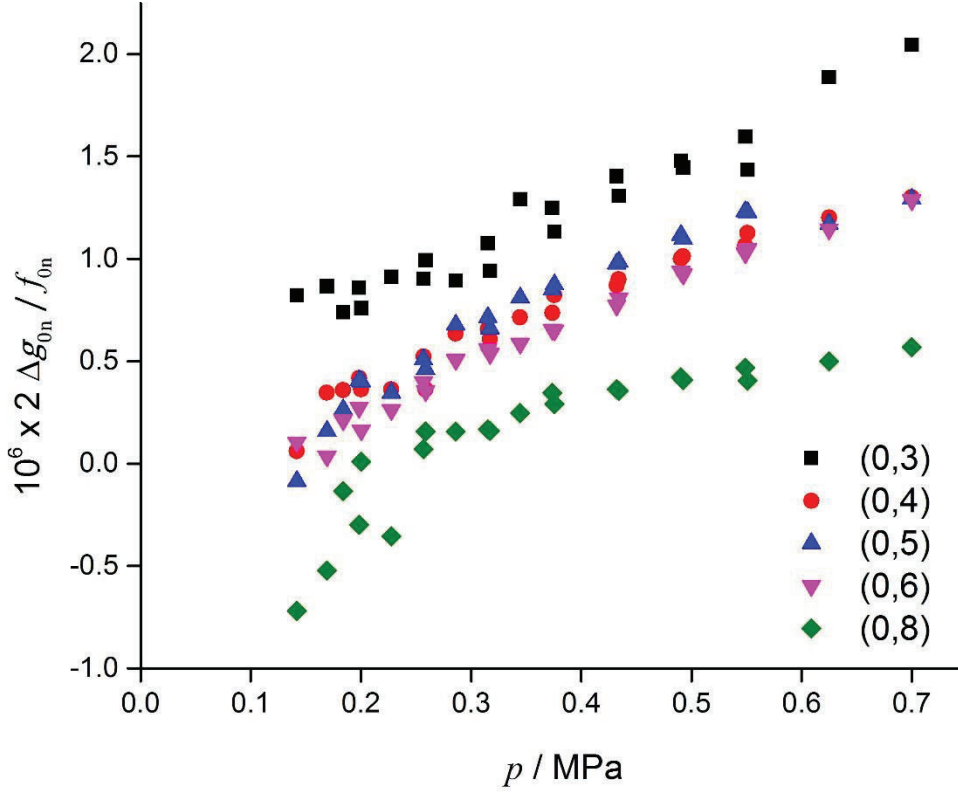


Figure 11. Double average excess half-widths $2\Delta g_{0n}$ relative to mode frequencies f_{0n} as a function of pressure for the ensemble of radial acoustic mode used to determine the Boltzmann constant. The fact the values lie close to zero gives confidence in the model used to analyze the acoustic resonance frequencies [8].

Finally, five acoustic modes are considered in the following for the determination of the Boltzmann constant: modes (0,3) to (0,6) and (0,8). As mentioned in the introduction, square acoustic velocities are fitted to a pressure-dependent function to yield values for the coefficients A'_0 , A_{-1} and A'_1 (equation (2)). There are at least three ways to do this to arrive at a final value for the A'_0 and thereby the Boltzmann constant. Values obtained using three methods described hereafter are given in Table 5 while further data is provided in appendix A. Method 1, used in previous experiments at LNE [8,10] and INRiM [14], determines the value of A_{-1} for each mode and uses these results to it to obtain a single mean estimate of the temperature jump coefficient ζ_T [44] (formerly the thermal accommodation coefficient h). This is then used to correct the frequency of each resonance and hence the speed of sound. The corrected data is then refitted with no A_{-1}/p term to yield individual values of A'_0 that are then averaged to give the result. According to the model, the relative frequency perturbation caused by imperfect thermal accommodation at the cavity surface is expected to be the same for all modes; moreover, it does not contribute to the halfwidths. In reality, the value of A_{-1} can include other effects that cause it to vary between modes. The drawback of Method 1 is thus that it neglects the experimental dispersion of the different acoustic modes, which should naturally lead to small variations between the fitted values of A_{-1} for each mode. Indeed, the intercepts of zero pressure extrapolations of excess half-widths do show tiny variations from one mode to another (figure 11). A second approach (Method 2), used notably by de Podesta *et al.* [23], is to constrain the values of A_{-1} and A'_0 to be identical for each mode in the fitting procedure. In this way, only fitted values of the A_{-1} coefficient vary from mode to mode, as one might expect. This method implies then the same assumptions as the first one, concerning both A'_0 and A_{-1} . A third possibility (Method 3) is to float all

three coefficients for each mode. The average value of A'_0 is then used to calculate k . The advantage of this method is that it includes and accounts for the experimental dispersion of different acoustic modes. However, to implement such a method successfully requires accurate acoustic data at low pressures; such data were not available in previous work [8,10]. While the uncertainties are somewhat greater than with the second method, it is no longer assumed that A_{-1} is mode-independent. For this reason, it is the one we chose to adopt for the determination of k . Results for the three methods are shown in appendix A. Whatever the relative merits of these approaches, it is most reassuring to note that they all yields values for k that agree to within their standard uncertainties. Figure 14 shows the residuals for all three methods.

Table 5 Values of coefficients A'_0 and their standard uncertainties $u_{A'0}$ obtained using three different methods of analysis of acoustic data. More details are given in appendix A.

Method	A'_0 ($\text{m}^2 \cdot \text{s}^{-2}$)	$u_{A'0}$ ($\text{m}^2 \cdot \text{s}^{-2}$)
1	0.13	0.08
2	0.16	0.15
3	0.09	0.27

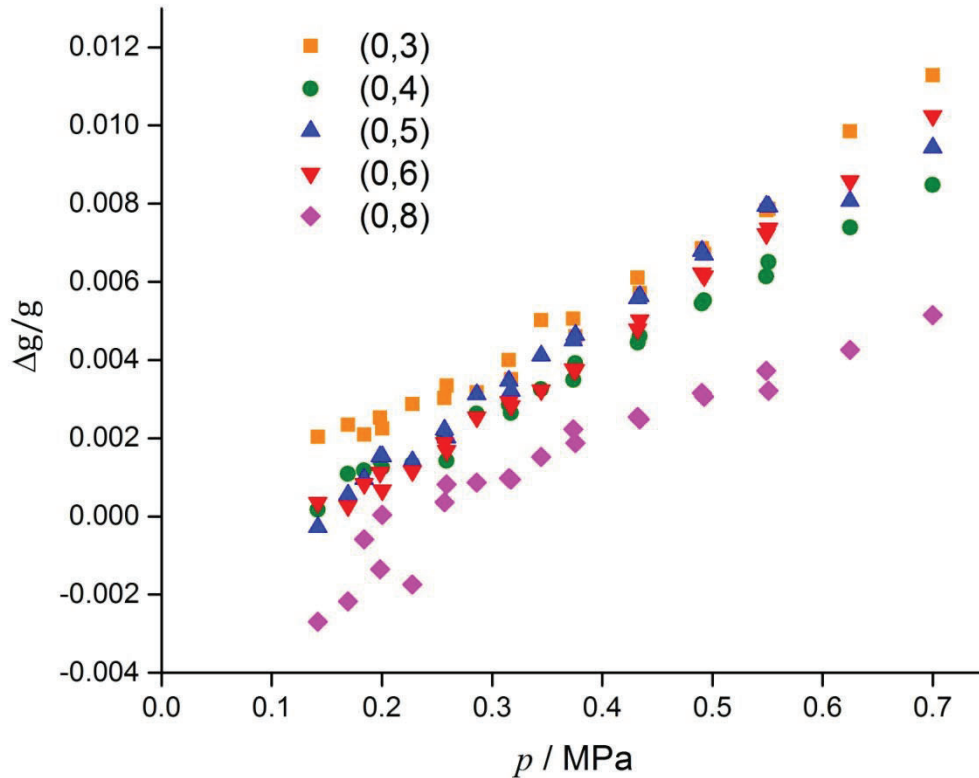


Figure 12. Plot of the function $\Delta g_{0n}/g_{0n}$ for the radial acoustic modes $(0, n)$ with $n=3, 4, 5, 6$ and 8 . The function describes the increase of the half-widths at low pressure due to thermal boundary layer losses. The convergence of all the intercepts towards zero indicates the good quality of the acoustic model at low pressure.

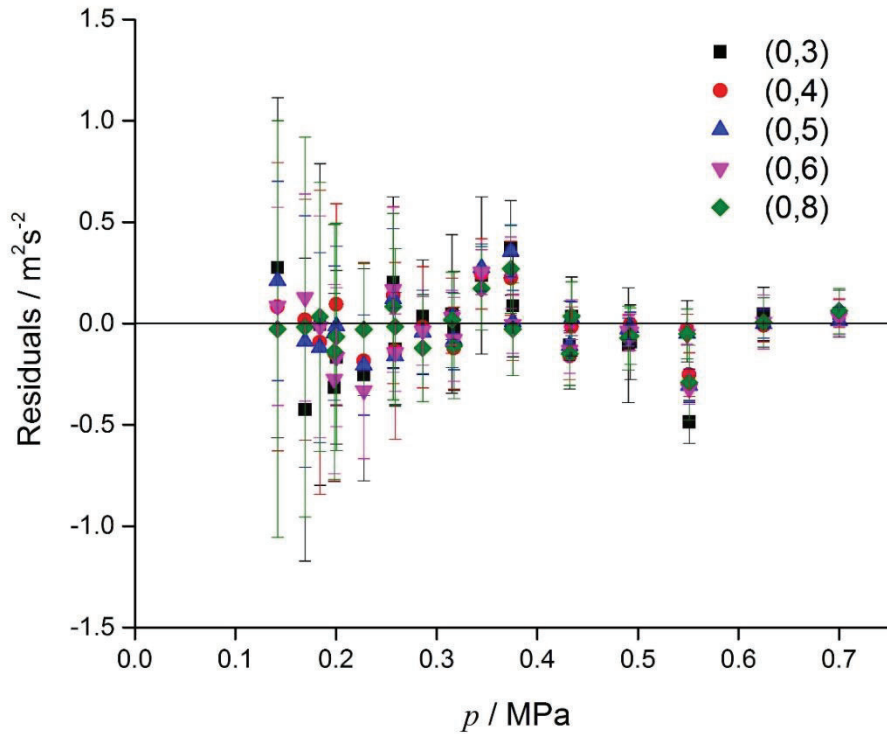


Figure 13. Residuals of the fits of the pressure-dependent function of equation (2) to selected acoustic data for five radial modes in the pressure range 0.15 MPa to 0.7 MPa. The error bars correspond to the type-A fitting uncertainty of each single datum shown previously in figures 8-10. The residuals obtained using the three different fitting methods described in the text are identical to the naked eye.

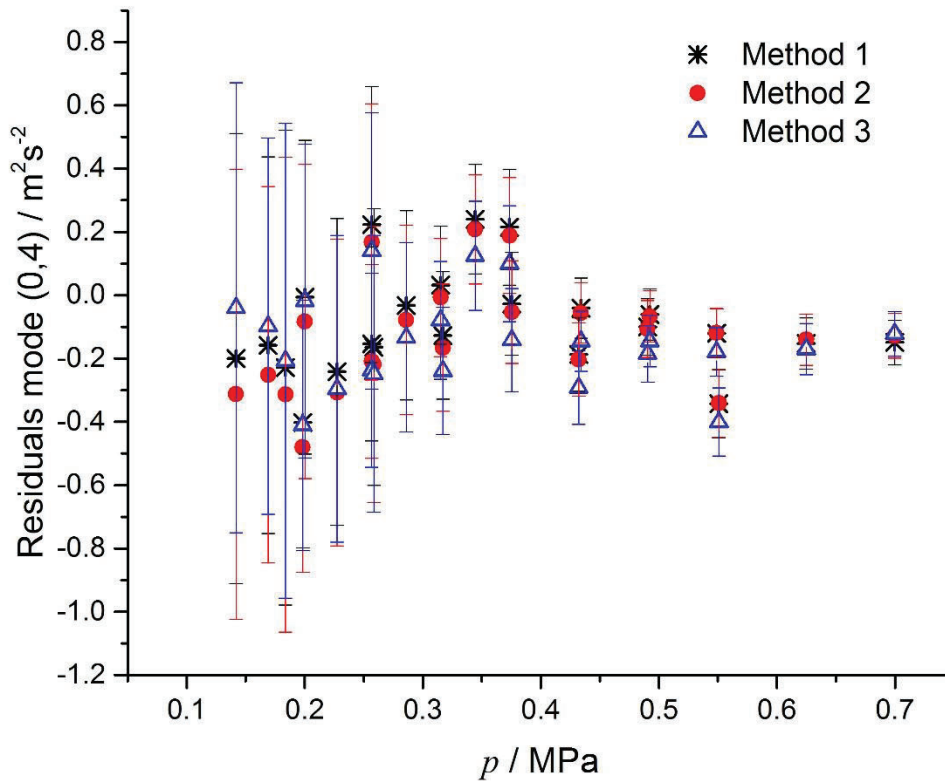


Figure 14. Residuals for fits of the square of the speed of sound for the radial mode (0,4) as a function of pressure deduced using Methods 1, 2 and 3 together with their standard uncertainties. The difference between the residuals of each method is clearly far less than the uncertainty, whatever the pressure.

7.4. Uncertainty budget for acoustic measurements

The uncertainty budget for acoustic measurements shown in Table 6 is dominated by two contributions. The largest of these, contributing to k at a level of 0.28×10^{-6} , results from the scatter among acoustic modes when the pressure-independent term of equation (2) is extracted. This scatter naturally includes the contribution due to the uncertainty in the frequency of each acoustic resonance from peak fitting. The guiding principle of acoustic thermometry is to use as many modes as possible to estimate this spread, itself an indication of the exactness of the acoustic model used. The second largest term, for which we have ascribed a conservative upper limit of 0.24×10^{-6} , arises from perturbations of the resonator surface due to the introduction of acoustic transducers. Although pressure measurements were made with particular care using a piston balance and servo control, there is some uncertainty in their value. This in turn has an impact on the analysis of acoustic frequencies as a function of pressure and contributions to the relative standard uncertainty in k at the level of 0.10×10^{-6} . An experimental limit on the effect of the tubing impedance yields a term of comparable size, namely 0.09×10^{-6} . There results a contribution of 0.06×10^{-6} from the *ab initio* value of the speed of sound arising from the uncertainty in the virial coefficients [12]. Finally, the two smallest contributions mentioned in the table, affecting k at the 0.02×10^{-6} level, are related to imperfect knowledge of the thermal conductivity of helium (via the boundary layer correction) and higher order corrections to allow for the non-spherical resonator shape. Assuming all these corrections to be independent, we calculate the total standard uncertainty as the square root of the quadratic sum, which amounts to 0.40×10^{-6} . It is therefore marginally the largest contributor to the total uncertainty in the Boltzmann constant, slightly exceeding the thermometry contribution discussed in section 3.

Table 6. Uncertainty budget for the acoustic measurements for the determination of the Boltzmann constant.

Term	Effect on k (Parts in 10^6)	Note
Scatter among modes	0.28	Disagreement among modes (0,3) to (0,6) and (0,8)
Thermal conductivity of helium	0.02	As given in [12]
Uncertainty of <i>ab initio</i> speed of sound	0.06	Due to uncertainty in <i>ab initio</i> virial coefficients
Microphone perturbation	0.24	Worst possible case
Relative shape perturbation corrections	0.02	Microwave or CMM eigenvalue
Tubing acoustic impedance	0.09	Difference in result when the impedance is increased by 10%
Pressure uncertainty	0.10	Offset of 11.2 Pa
Total	0.40	Square root of the sum of squares

8. Final result and uncertainty budget

We find a value for the universal gas constant $R=8.314\,4614\,(50)\text{ J}\cdot\text{mol}^{-1}\cdot\text{K}^{-1}$. Using the current best available value of the Avogadro constant $N_A=6.022140857(74)\times 10^{23}\text{ mol}^{-1}$ [7], we obtain $k=1.38064878\,(83)\times 10^{-23}\text{ J}\cdot\text{K}^{-1}$. Figure 10 shows the present result along with other measurements of the Boltzmann constant including CODATA 2014. Overall the most recent determinations by non-acoustic techniques have uncertainties at the level of the earlier acoustic measurements and are in general agreement with them. We see our value lies close to the CODATA 2014 value and is in good agreement with that of our previous determinations. The overall uncertainty, below 1 part in 10^6 includes the contributions of acoustic measurements, thermometry and pressure determinations, dimensional size and mass spectrometry. One of the largest components, 0.39parts in 10^6 , was from the thermometry. The budget is given in Table 1. Upon request, the authors will provide the data in the form of spreadsheets. Also, the data will be posted on the internet [45]. In all our experiments, the uncertainty contributions related to resonator size, molar mass and temperature are correlated to a certain extent. In appendix B, we examine the effect of such correlations on the weighted average of all our measurements, which should be of interest to CODATA.

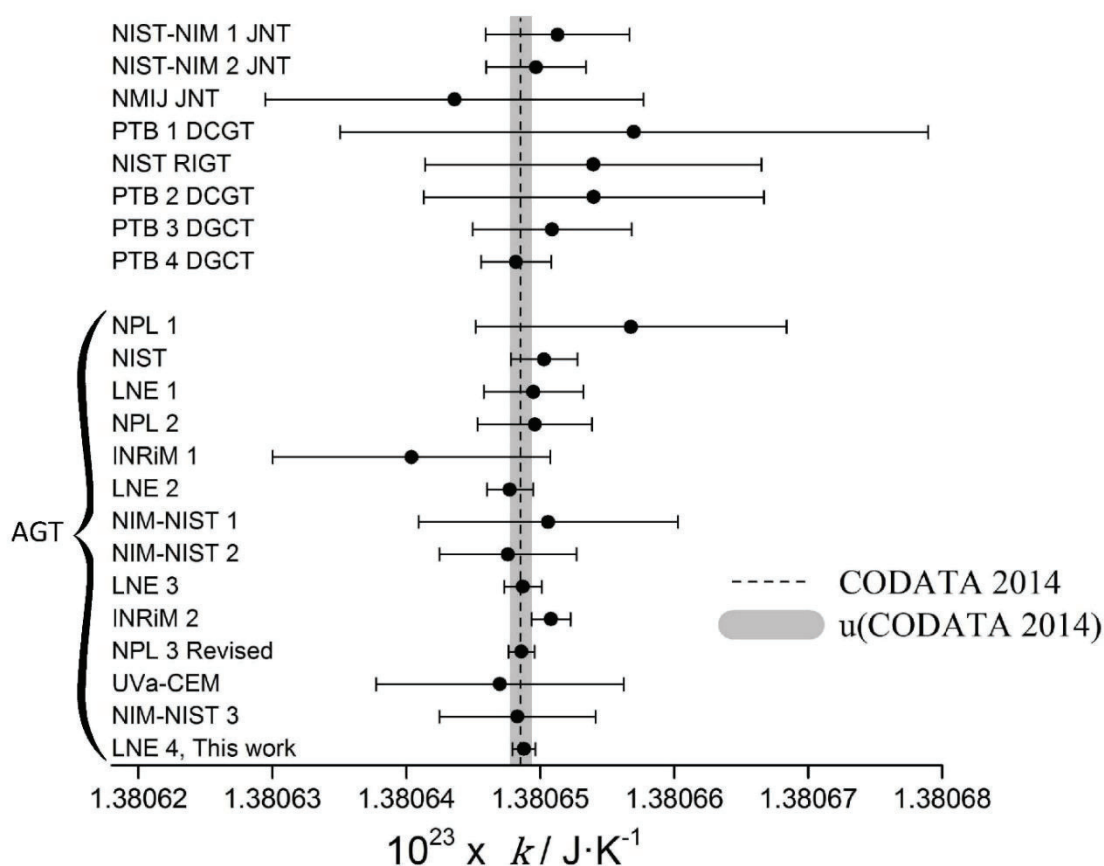


Figure 15. Determinations of the Boltzmann constants showing values and their standard uncertainties. The present result LNE4 lies in excellent agreement with the CODATA 2014 value and is compatible with results of our previous determinations of k . For clarity, we have separated results obtained using AGT (AGT) from those from dielectric constant gas thermometry (DCGT), Johnson noise thermometry (JNT) and refractive-index gas thermometry (RIGT); chronological order within each group is from top to bottom; References: CODATA 2014 [7], NPL1 [46], NPL2 [31], NPL3 [23] corrected in [47] and [48], INRiM1 [15], INRiM2 [14], LNE1 [9], LNE2 [8], LNE2 [10], NIM-NIST1 [49], NIM-NIST2 [50], NIM-NIST 3 [51] NIST JNT 1 [52], NIST JNT 2 [53], NIST RIGT [54], PTB1 [55], PTB2 [56], PTB3 [57], PTB4 [58] NMIJ-JNT[59] UVa-CEM [60].

9. Conclusion and perspectives

We have performed a new measurement of the Boltzmann constant k by acoustic thermometry of helium-4 gas. It marks an improvement in accuracy over our previous measurement using a smaller resonator of similar design. The result is in good agreement with our previous measurement with helium [10] and consistent with that performed with helium by Gavioso *et al* [14] in a resonator of volume 3-litres. We believe the lower data scatter and corresponding lower uncertainty components for acoustic and microwave measurements result from a better-defined geometry of the tri-axial ellipsoid (here) compared with that of two slightly offset hemispheres (Gavioso *et al* [14]). In our case, it was possible to use higher-order shape corrections calculated by Mehl [25,26] that were essential to obtain the stated level of accuracy. The present result also agrees with that of our earlier measurements of k using argon [8,9]. All our measurements yield values close to the CODATA 2014 value [7] derived from many determinations including those using other techniques (*e.g.* DCGT).

Perhaps the most interesting aspect of the present work lies in the analysis of acoustic resonances and their associated correction terms. For modes whose frequencies lie closest to those of shell vibrations, there is clearly a pressure-dependent effect. Reducing the effect of the shell vibrations is straightforward to implement and should be of future benefit in all similar acoustic gas thermometry experiments worldwide.

Acknowledgments

We acknowledge helpful discussions with colleagues in our own institute and elsewhere, especially, A-M Bruneau, M Bruneau, Xiaojuan Feng, C Gaiser, R Gavioso, K Gillis, G Sutton, R Underwood and Jintao Zhang. We are grateful to R Berg for many helpful discussions and fruitful exchanges. We are deeply grateful to I Yang for providing valuable information on isotopic analysis at short notice. We thank both referees for their invaluable remarks that greatly improved the quality of the manuscript. We are grateful to D Truong, A Vergé, B Buée and A Richard who provided vital input during the design stages and the assembly of the resonator and D Bentouati, P Otal and P Gambette for calibration of the piston balance pressure gauge. B Andasse contributed to the ensemble of LNE measurements in ways too numerous to mention. The international collaboration from which this experiment benefitted owes much to M Chambon of LNE. In addition, these results would not have been obtained without the support of TJ Quinn, F Le Frious, F Platel and Y Hermier. We gratefully acknowledge funding from the French National Research Agency ANR and the EURAMET Joint Research Project which receives funding from the European Union's Seventh Framework programme under Grant Agreement n° 217257.

Appendix A: Values of coefficients A'_0 , A'_{-1} and their standard uncertainties obtained using three different methods of analysis of acoustic data.

Values of coefficients obtained using Method 1 are shown in Table A1. The Method yielded a value of the thermal jump coefficient $\zeta_T = 6.740$ ($h=0.395$). The weighted average $A'_0 = 0.13$ ($\text{m}^2 \cdot \text{s}^{-2}$) with an uncertainty of 0.084 ($\text{m}^2 \cdot \text{s}^{-2}$).

Table A1. Values of the coefficients A'_0 , A'_{-1} and their respective standard uncertainties $U_{A'_0}$ and $U_{A'_1}$ obtained using Method 1 for the radial acoustic modes (0,3) to (0,6) and (0,8).

Radial acoustic mode	A'_0 ($\text{m}^2 \cdot \text{s}^{-2}$)	$U_{A'_0}$ ($\text{m}^2 \cdot \text{s}^{-2}$)	A'_1 ($\text{m}^2 \cdot \text{s}^{-2} \cdot \text{MPa}^{-1}$)	$U_{A'_1}$ ($\text{m}^2 \cdot \text{s}^{-2} \cdot \text{MPa}^{-1}$)
(0,3)	0.15	0.30	91.84	0.24
(0,4)	0.18	0.27	31.02	0.22
(0,5)	0.12	0.20	18.76	0.16
(0,6)	0.09	0.21	13.75	0.17
(0,8)	0.17	0.29	9.21	0.23

Values of coefficients obtained using Method 2 are shown in Table A2. From the value of A'_{-1} , we obtain $\zeta_T = 6.65 \pm 0.67$ while the value of $A'_0 = -0.051$ ($\text{m}^2 \cdot \text{s}^{-2}$) with an uncertainty of 0.145 ($\text{m}^2 \cdot \text{s}^{-2}$).

Table A2. Values of the coefficients A'_0 , A'_{-1} , A'_{13} , A'_{14} , A'_{15} , A'_{16} and A'_{18} obtained using Method 2 together with their respective standard uncertainties. The subscript "13" refers to the coefficient A'_1 for radial mode (0,3) etc.

Coefficient	Value	Standard uncertainty
A'_0 ($\text{m}^2 \cdot \text{s}^{-2}$)	0.160	0.145
A'_{-1} ($\text{m}^2 \cdot \text{s}^{-2} \cdot \text{MPa}$)	1.395	0.03
A'_{13} ($\text{m}^2 \cdot \text{s}^{-2} \cdot \text{MPa}^{-1}$)	91.76	0.16
A'_{14} ($\text{m}^2 \cdot \text{s}^{-2} \cdot \text{MPa}^{-1}$)	31.11	0.17
A'_{15} ($\text{m}^2 \cdot \text{s}^{-2} \cdot \text{MPa}^{-1}$)	18.76	0.17
A'_{16} ($\text{m}^2 \cdot \text{s}^{-2} \cdot \text{MPa}^{-1}$)	13.47	0.17
A'_{18} ($\text{m}^2 \cdot \text{s}^{-2} \cdot \text{MPa}^{-1}$)	9.31	0.17

Values of coefficients obtained using Method 3 are shown in Table A3. They yield a weighted average $A'_0 = 0.16$ ($\text{m}^2 \cdot \text{s}^{-2}$) with an uncertainty of 0.27 ($\text{m}^2 \cdot \text{s}^{-2}$).

Table A3. Values of the coefficients A'_0 , A'_1 and the thermal jump coefficient ζ_T together with their standard uncertainties obtained using Method 3 for the radial modes (0,3) to (0,6) and (0,8).

Radial acoustic mode	A'_0 ($\text{m}^2 \cdot \text{s}^{-2}$)	$u_{A'_0}$ ($\text{m}^2 \cdot \text{s}^{-2}$)	A'_1 ($\text{m}^2 \cdot \text{s}^{-2} \cdot \text{MPa}^{-1}$)	$u_{A'_1}$ ($\text{m}^2 \cdot \text{s}^{-2} \cdot \text{MPa}^{-1}$)	ζ_T	u_{ζ_T}
(0,3)	0.59	0.46	91.24	0.20	6.481	0.46
(0,4)	-0.54	0.41	31.87	0.18	7.10	0.41
(0,5)	0.11	0.30	18.84	0.13	6.773	0.31
(0,6)	0.38	0.32	13.17	0.14	6.486	0.33
(0,8)	0.20	0.46	9.37	0.19	6.808	0.46

Appendix B: Average of all four determinations of k at LNE with or without correlation

The LNE group has made four measurements of the Boltzmann constant k by acoustic thermometry one with argon “LNE 2” [8], and three with helium-4 “LNE1” [9] “LNE 3” [10] and this work “LNE 4”. They used three different quasi-spherical ellipsoidal resonators. The first “kBCU2v2” had a volume of 0.5 litre but its surface was not diamond turned. The second, “kBCU3” also of volume 0.5 l had a diamond turned surface. The third “kBCU4” used in the present experiment has a volume around 3 l and a diamond-turned surface. These measurements are correlated to a certain degree since they involve some of the same apparatus for measuring temperature, molar mass and the resonator’s dimensions. Since it is not possible for us to specify the exact values of correlation coefficients, we treat the limiting cases to obtain weighted averages of the four values.

The first two experiments using helium then argon had different resonators (kBCU2v2 and kBCU3) but the same thermometers so only thermometry could have been correlated. The latter resonator and thermometers were the same as those used for the second experiment with helium-4 (kBCU3He). In the experiments on helium, the molar mass determinations could be correlated. In fact, different laboratories performed the mass spectrometry for the helium experiments (LNE 3 and LNE 4) so we are conservative by assuming that these mass determinations are correlated. The correlations shown in Table B1 were included or not (with a correlation coefficient of 1 if correlated and 0 if not).

Table B1. Correlation of parameters between the four determinations of the Boltzmann constant k carried out at LNE: T =temperature, M = molar mass, a = effective radius.

Experiment	LNE 1	LNE 2	LNE 3	LNE 4
LNE 1		T	T, M	T, M
LNE 2	T		T, a	T
LNE 3	T, M	T, a		T, M
LNE 4	T, M	T	T, M	

To obtain the value of Boltzmann’s constant shown in Tables B2 and B3, we used the CODATA 2006 [61] value of the Avogadro constant and the atomic weights for the experiments LNE 1 and LNE 2, the CODATA 2010 [62] value for LNE 3 and that of CODATA 2014 [7] for the present measurement LNE 4.

Table B2. Values of standard uncertainties and relative weights r for the four determinations of the Boltzmann constant k at LNE. The negative value for LNE1 is the result of a numerical accident.

Experiment	Gas	Resonator	$k \times 10^{23}$ (J.K ⁻¹)	u_r (Parts in 10 ⁶)	r (without)	r (with)	Reference
LNE1	He	kBCU2v2	1.3806496	2.79	0.03	-0.01	[9]
LNE 2	Ar	kBCU3	1.3806477	1.40	0.11	0.08	[8]
LNE 3	He	kBCU3	1.3806487	1.04	0.21	0.13	[10]
LNE 4	He	kBCU4	1.38064878	0.60	0.65	0.80	This work
k (without)			1.38064887	0.48			
k (with)			1.38064887	0.56			

The negative value for LNE 1 arises from the inverse matrix of the correlation matrix. Note that this experiment has a much greater standard uncertainty than the three others. It is interesting therefore to consider the result with the analysis limited to the last three determinations of k (Table B3). When correlations are included, the ensemble average has the same uncertainty as that of the average of all four experiments, namely 0.56 parts in 10^6 . With no correlations, the ensemble average of the four measurements has an uncertainty marginally lower (0.48 parts in 10^6) than that with three (0.49 parts in 10^6). This implies that including or ignoring LNE1 will have a negligible impact on the final value of k used for the future definition of the kelvin.

Table B3. Values of the Boltzmann constant and universal gas constant together with their standard uncertainties and relative weights r for the last three determinations of the Boltzmann constant k at LNE. Due to the negligible uncertainty of the Avogadro constant, the relative uncertainty in k and R is identical at this level of accuracy.

Experiment	$k \times 10^{23}$ (J.K ⁻¹)	R (J.mol ⁻¹ .K ⁻¹)	u_R (Parts in 10^6)	r (without)	r (with)
LNE 2	1.3806477	8.3144565	1.40	0.12	0.08
LNE 3	1.3806487	8.3144615	1.04	0.21	0.13
LNE 4	1.38064878	8.31446142	0.60	0.67	0.79
k (without)	1.38064864	8.31446084	0.49		
k(with)	1.38064868	8.31446102	0.56		

The values of k in Tables B2 and B3 (and in the supporting publications) used the best values of the Avogadro constant and atomic weights available at the time of publication. For the convenience of the CODATA group and others who would like to recalculate k , we provide the values of the squared speed of sound c_0^2 and molar mass for each of our four determinations. These are given in Table B4 together with their standard uncertainties.

Table B4. Values of the squared speed of sound and molar mass of helium-4 (LNE 1, LNE 2 and LNE 4) and argon (LNE3) together with their standard uncertainties. The molar mass uncertainty of LNE 2 was changed according to [47].

Experiment	c_0^2 (m.s ⁻¹)	$u_{c_0^2}$ (m.s ⁻¹)	M (g.mol ⁻¹)	u_M (g.mol ⁻¹)
LNE1	945709.4	2.2	4.00260325	9.6×10^{-7}
LNE 2	94756.01	0.1	39.947805	3.5×10^{-5}
LNE 3	945708.82	0.79	4.0026032	2.1×10^{-6}
LNE 4	945708.81	0.42	4.00260321	3.6×10^{-7}

References

- [1] *Comptes rendus des séances de la Treizième Conférence Générale des Poids et Mesures* (Paris 10-16 Oct 1967 and 15 Oct 1968) (Sevres: BIPM)
(www.bipm.org/utis/common/pdf/CGPM/CGPM13.pdf)
- [2] Stock M *et al* 2006 CCT-K7: Key comparison of water triple point cells report B *Metrologia* **43** 03001
- [3] Mills I M, Mohr P J, Quinn T J, Taylor B N and Williams E R 2005 Redefinition of the kilogram, ampere, kelvin and mole: a proposed approach to implementing CIPM recommendation 1 (CI-2005) *Metrologia* **43** 227–46
- [4] Fischer J and Ullrich J 2016 The new system of units *Nat. Phys.* **12** 4–7
- [5] Moldover M R, Gavioso R M, Mehl J B, Pitre L, de Podesta M and Zhang J T 2014 Acoustic gas thermometry *Metrologia* **51** R1–19
- [6] Gaiser C, Zandt T and Fellmuth B 2015 Dielectric-constant gas thermometry *Metrologia* **52** S217–26
- [7] Mohr P J, Newell D B and Taylor B N 2016 CODATA recommended values of the fundamental constants: 2014 *Rev. Mod. Phys.* **88** 035009
- [8] Pitre L, Sparasci F, Truong D, Risegari L, Guillou A and Himbert M 2011 Measurement of the Boltzmann constant k_B using a quasi-spherical acoustic resonator *Int. J. Thermophys.* **32** 1825–86
- [9] Pitre L, Guianvarc’h C, Sparasci F, Guillou A, Truong D, Hermier Y and Himbert M E 2009 An improved acoustic method for the determination of the Boltzmann constant at LNE-INM/CNAM *C. R. Phys.* **10** 835–48
- [10] Pitre L, Sparasci F, Risegari L, Plimmer M D, Himbert M E and Giuliano Albo P A 2015 Determination of the Boltzmann constant k from the speed of sound in helium gas at the triple point of water *Metrologia* **52** S263–73
- [11] Moldover M R, Trusler J P M, Edwards T J, Mehl J B and Davis R S 1988 Measurement of the universal gas constant R using a spherical acoustic resonator *J. Res. Natl. Bur. Stand.* **93** 85–144
- [12] Cencek W, Przybytek M, Komasa J, Mehl J B, Jeziorski B and Szalewicz K 2012 Effects of adiabatic, relativistic, and quantum electrodynamics interactions on the pair potential and thermophysical properties of helium *J. Chem. Phys.* **136** 224303
- [13] Garberoglio G, Moldover M R and Harvey A H 2011 Improved first principles calculation of the third virial coefficient of helium *J. Res. Nat. Inst. Stand. Technol.* **116** 729–42
- [14] Gavioso R M, Madonna Ripa D, Steur P P M, Gaiser C, Truong D, Guianvarc’h C, Tarizzo P, Stuart F M and Dematteis R 2015 A determination of the molar gas constant R by acoustic thermometry in helium *Metrologia* **52** S274–304
- [15] Gavioso R M, Giuliano Albo P A, Madonna Ripa D, Merlone A, Guianvarc’h C, Moro F and Cuccaro R 2010 A determination of the Boltzmann constant from speed of sound measurements in helium at a single thermodynamic state *Metrologia* **47** 387–409

- [16] Pitre L, Sparasci F, Risegari L, Guianvarc'h C, Plimmer M D and Himbert M E 2014 Improved apparatus to determine the Boltzmann constant using a large quasi-spherical acoustic resonator 29th Conf. on Precision Electromagnetic Measurements (Rio de Janeiro, Brazil, 24–29 August 2014) Poster
- [17] Gillis K A, Mehl J B, Schmidt J W and Moldover M R 2015 Weighing a gas with microwave and acoustic resonances *Metrologia* **52** 337–52
- [18] Mabry J, Lan T F, Burnard P G and Marty B 2013 High-precision helium isotope measurements in air *J. Anal. At. Spectrom.* **28** 1903–10
- [19] Mabry J C, Lan T, Boucher C, Burnard P G, Brennwald M S, Langenfelds R and Marty B 2015 No evidence for change of the atmospheric helium isotope composition since 1978 from re-analysis of the Cape Grim Air Archive *Earth Planet. Sci. Lett.* **428** 134–8
- [20] Yoshiki H, Nakai H and Gutsmedl E 2005 A new superleak to remove He 3 for UCN experiments *Cryogenics* **45** 399–403
- [21] Ballentine C J, Burgess R and Marty B 2002 Tracing fluid origin, transport and interaction in the crust *Rev. Mineral. Geochem.* **47** 539–614
- [22] Purer A, Stroud L and Meyer T O 1965 Simple technique for the ultrapurification of helium *Advances in Cryogenic Engineering* vol 10, ed K D Timmerhaus (New York:Plenum) pp 398–401
- [23] de Podesta M, Underwood R, Sutton G, Morantz P, Harris P, Mark D F, Stuart F M, Vargha G and Machin G 2013 A low uncertainty measurement of the Boltzmann constant *Metrologia* **50** 354–76
- [24] Underwood R J, Mehl J B, Pitre L, Edwards G, Sutton G and de Podesta M 2010 Waveguide effects on quasi spherical microwave cavity resonators *Meas. Sci. Technol.* **21** 075103
- [25] Mehl J B 2009 Second-order electromagnetic eigenfrequencies of a triaxial ellipsoid *Metrologia* **46** 554–9
- [26] Mehl J B 2015 Second-order electromagnetic eigenfrequencies of a triaxial ellipsoid II *Metrologia* **52** S227–32
- [27] Piszczatowski K, Puchalski M, Jacek Komasa J, BogumiłJeziorski B and Szalewicz K 2015 Frequency-dependent polarizability of helium including relativistic effects with nuclear recoil terms *Phys. Rev. Lett.* **114** 173004
- [28] Cencek W, Komasa J and Szalewicz K 2011 Collision-induced dipole polarizability of helium dimer from explicitly correlated calculations *J. Chem. Phys.* **135** 014301
- [29] de Podesta M, May E F, Mehl J B, Pitre L, Gaviolo R M, Benedetto G, Giuliano Albo P A, Truong D and Flack D 2010 Characterization of the volume and shape of quasi-spherical resonators using coordinate measurement machines *Metrologia* **47** 588–604
- [30] Pitre L, Moldover M R and Tew W L 2006 Acoustic thermometry: new results from 273 K to 77 K and progress towards 4 K *Metrologia* **43** 142–62
- [31] Sutton G, Underwood R, Pitre L, de Podesta M and Valkiers S 2010 Acoustic resonator experiments at the triple point of water: first results for the Boltzmann constant and remaining challenges *Int. J. Thermophys.* **31** 1310–46
- [32] Guianvarc'h C, Pitre L, Bruneau A-M and Bruneau M 2009 Acoustic field in a quasi-spherical resonator: unified perturbation model *J. Acoust. Soc. Am.* **125** 1416–25

- [33] Guianvarc'h C, Gavioso R, Benedetto G, Pitre L and Bruneau M 2009 Characterization of condenser microphones under different environmental conditions for accurate speed of sound measurements with acoustic resonators *Rev. Sci. Instrum.* **80** 074901
- [34] Mehl J B, Moldover M R and Pitre L 2004 Designing quasi-spherical resonators for acoustic thermometry *Metrologia* **41** 295–304
- [35] Moldover M R, Mehl J B and Greenspan M 1986 Gas-filled spherical resonators—theory and experiment *J. Acoust. Soc. Am.* **79** 253–72
- [36] Moldover M R, Gavioso R M and Newell D B 2015 Correlations among acoustic measurements of the Boltzmann constant *Metrologia* **52** S376–84
- [37] Rodrigues D, Guianvarc'h C, Durocher J-N, Bruneau M and Bruneau A-M 2008 A method to measure and interpret input impedance of small acoustic components *J. Sound Vib.* **315** 890–910
- [38] Gillis K A, Lin H and Moldover M R 2009 Perturbations from ducts on the modes of acoustic thermometers *J. Res. Natl Inst. Stand. Technol.* **114** 263–85
- [39] Levine H and Schwinger J 1947 On the radiation of sound from an unflanged circular pipe *Phys. Rev.* **73** 383–406
- [40] Bruneau M, Bruneau A-M, Škvor Z and Lotton P 1994 An equivalent network modelling the strong coupling between a vibrating membrane and a fluid film *Acta Acust.* **2** 223–32
- [41] Zuckerwar A J 1978 Theoretical response of condenser microphones *J. Acoust. Soc. Am.* **64** 1278–85
- [42] Gillis K A 2012 Second-order boundary corrections to the radial acoustic eigenvalues for a spherical cavity *Metrologia* **49** L21–4
- [43] Mehl J B 1985 Spherical acoustic resonator: effects of shell motion *J. Acoust. Soc. Am.* **78** 782–8
- [44] Sharipov F and Moldover M R 2016 Energy accommodation coefficient extracted from acoustic resonator experiments *J. Vac. Sci. Technol. A* **34** 061604
- [45] <http://lcm.cnam.fr/thermometrie/kb.helium.2017.zip>
- [46] Colclough A R, Quinn T J and Chandler C T R 1979 An acoustic redetermination of the gas constant *Proc. R. Soc. A* **368** 125–39
- [47] Yang I, Pitre L, Moldover M R, Zhang J T, Feng X J and Kim J S 2015 Improving acoustic determinations of the Boltzmann constant with mass spectrometer measurements of the molar mass of argon *Metrologia* **52** S394–409
- [48] de Podesta M, Mark D F, Dymock R C, Underwood R, Bacquart T, Sutton G, Davidson S and Machin G 2017 Re-estimation of argon isotope ratios leading to a revised estimate of the Boltzmann constant *Metrologia* **54** 683
- [49] Zhang J T, Lin H, Sun J P, Feng X J, Gillis K A and Moldover M R 2010 Cylindrical acoustic resonator for the re-determination of the Boltzmann constant *Int. J. Thermophys.* **31** 1273–93

- [50] Zhang J T, Lin H, Feng X J, Sun J P, Gillis K A, Moldover M R and Duan Y Y 2011 Progress toward redetermining the Boltzmann constant with a fixed-path-length cylindrical resonator *Int. J. Thermophys.* **32** 1297–329
- [51] Feng X J, Zhang J T, Lin H, Gillis K A, Mehl J B, Moldover M R, Zhang K and Duan Y N 2017 Determination of the Boltzmann constant with cylindrical acoustic gas thermometry: new and final results *Metrologia* **54** 748
- [52] Qu J, Benz P, Pollarolo A, Rogalla H, Tew W L, White R and Zhou K 2015 Improved electronic measurement of the Boltzmann constant by Johnson noise thermometry *Metrologia* **52** S242–56
- [53] Qu J, Benz S P, Coakley K, Rogalla H, Tew W L, White R, Zhou K and Zhou Z 2017 An improved electronic determination of the Boltzmann constant by Johnson noise thermometry *Metrologia* **54** 549
- [54] Schmidt J W, Gavioso R M, May E F and Moldover M R 2007 Polarizability of helium and gas metrology *Phys. Rev. Lett.* **98** 24504
- [55] Gaiser C, Fellmuth B and Haft N 2008 Primary dielectric-constant gas thermometry in the range from 2.4 K to 26 K at PTB *Int. J. Thermophys.* **29** 18–30
- [56] Fellmuth B, Fischer J, Gaiser C, Jusko O, Prieruenrom T, Sabuga W and Zandt T 2011 Determination of the Boltzmann constant by dielectric-constant gas thermometry *Metrologia* **48** 382–90
- [57] Gaiser C, Zandt T, Fellmuth B, Fischer J, Jusko O and Sabuga W 2013 Improved determination of the Boltzmann constant by dielectric-constant gas thermometry *Metrologia* **50** L7–11
- [58] Gaiser C, Fellmuth B, Haft N, Kuhn A, Thiele-Krivoi B, Zandt T, Fischer J, Jusko O and Sabuga W 2017 Final determination of the Boltzmann constant by dielectric-constant gas thermometry *Metrologia* **54** 280–9
- [59] Urano C, Yamazawa K and Kaneko N-H 2017 Measurement of the Boltzmann constant by Johnson noise thermometry using superconducting integrated circuit *Metrologia* **52** 847–55
- [60] Segovia J J, Lozano-Martín D, Martín M C, Chamorro C R, Villamañán M A, Pérez E, García Izquierdo C, and del Campo D 2017 Updated determination of the molar gas constant R by acoustic measurements in argon at UVa-CEM *Metrologia* **54** 663
- [61] Mohr P J, Taylor B N and Newell D B 2008 CODATA recommended values of the fundamental physical constants:2006 *Rev. Mod. Phys.* **80** 633–730
- [62] Mohr P J, Taylor B N and Newell D B 2012 CODATA recommended values of the fundamental physical constants:2010 *Rev. Mod. Phys.* **84** 1527–605